Layer-by-layer resolved core-level shifts in CaF_2 and SrF_2 on Si(111): Theory and experiment

Eli Rotenberg*,†
Department of Physics, University of California, Berkeley, California 94720

J. D. Denlinger*
Department of Physics, University of Wisconsin, Milwaukee, Wisconsin 53211

M. Leskovar, U. Hessinger, and Marjorie A. Olmstead
Department of Physics, FM-15, University of Washington, Seattle, Washington 98195
(Received 23 February 1994)

Using x-ray-photoelectron spectroscopy and Auger-electron spectroscopy, we have resolved surface, bulk, and interface Ca and F core-level emission in thin films (3–8 triple layers) of CaF_2 and SrF_2 on Si(111). We confirmed these assignments using x-ray-photoelectron diffraction (XPD) and surface modification. XPD was also used to identify the growth modes of the films as being either laminar or layer plus islands; in the latter case we have resolved buried and uncovered interface F and Ca/Sr emission. We compare the observed energy differences between surface, bulk, and interface emission to theoretical estimates of the extra-atomic contributions to emission energies. We find excellent agreement considering only the Madelung (electrostatic) potentials for the initial-state contribution and polarization response for the final-state contribution, including the effect of tetragonal strain. Small discrepancies for emission from metal atoms bonded to the Si substrate are interpreted in terms of chemical shifts.

I. INTRODUCTION

Variations in core-level energies, as measured by x-ray-photoelectron spectroscopy (XPS) and Auger-electron spectroscopy (AES), yield important information about the surfaces and interfaces of materials.[1–3] In the customary picture, core-level energy shifts are directly related to the chemical state of the photoemitting atom. However, the geometric (extra-atomic) factors which contribute to core-level energies can also be important for some solids. In this paper, we examine in detail the relationship between known geometry and observed core-level shifts (CLS's) for the strongly ionic insulators CaF_2 and SrF_2. By geometry, we are referring to the atomic arrangement near a given atom and its alteration near abrupt surfaces and interfaces. These structural properties give rise to extra-atomic contributions to CLS's.

Surface and interface photoemission and Auger-energy shifts (collectively referred to as CLS's) arise from a number of causes. In addition to the broad division into chemical (intra-atomic) and geometric (extra-atomic) effects, contributions to core-level shifts may also be divided into initial- and final-state energies. In this paper, we present a model for the initial- and final-state extra-atomic contributions for thin ionic solid films and compare the resulting theoretical CLS's with experiment for CaF_2 and SrF_2 on Si(111). Discrepancies between theory and experiment then set a limit on the residual chemical, or intra-atomic effects. We principally concentrate on surface CLS's (SCLS's) of ionic insulators, because at these surfaces the geometric arrangements are abruptly altered while the chemical states of the surface atoms are often bulklike.

The geometric contributions to CLS's are easily modeled for a given atomic structure. The initial-state energy is determined by the electrostatic potential acting on an electron before it is emitted from the solid; the principal extra-atomic contribution to this energy in ionic crystals is the long-range Madelung (electrostatic) potential due to the arrangement of ions in the solids of interest.[4–7] The final-state energy is determined by the relaxation of the solid's electronic orbitals just after the sudden creation of the core hole; the principal extra-atomic contribution is the polarization response of the neighboring atoms.[4,5,8–10] We model the final state with no charge transfer from neighboring atoms,[11] as proposed by Veal and Paulikas.[12] Other extra-atomic effects (the repulsion due to overlap with neighboring atoms, van der Waals forces, etc.[5]) are assumed to be the same for all the different atomic sites in the crystal.

Previously, we have used the final-state model to reproduce experimental CLS's in insulating rare-gas solids on metal substrates, where the simple van der Waals bonding precludes any initial-state effects.[13] We showed that the final-state energy shift is of comparable magnitude to the initial-state contribution (even for strongly ionic crystals), and it can even cancel out the initial-state shift for specific structures. Thus, inclusion of the final-state effect is important when interpreting the chemical state of surface species from their SCLS's. This improves upon previous work which only included the initial-state shift in the interpretation of SCLS's.[7,14–18]

CaF_2 and SrF_2 are excellent prototypes for studying the relationship between structure and core-level shifts,

since considerable progress has been made towards understanding their epitaxy on Si(111) substrates. Additionally, their (111) surfaces have simple bulk termination,[19–21] and synchrotron radiation studies of the valence bands of fluorides on Si(111) indicate no metallic character.[22–24] This suggest that the surface and bulk charge transfers are identical, so that little chemical, or intra-atomic, effects are found at the surface. Consequently, studies of SCLS's in these materials test models for the extra-atomic effects on observed core-level energies.

SrF_2, CaF_2, and Si have similar face-centered-cubic structures; CaF_2 (SrF_2) has a room-temperature lattice constant 0.6% (6.8%) larger than Si. In thin films of MF_2 (where M =Ca or Sr) on Si(111), the interface is nonstoichiometric; i.e., the interface consists of a chemically reacted Si-M-F layer, with subsequent growth of stoichiometric F-M-F triple layers (TL's).[25,26] (Even though the interface is missing a layer of F atoms, we still refer to the Si-M-F layer as a TL.) Figure 1 shows a model of the MF_2 on the Si(111) system, along with labels used for the different atomic sites. We do not probe the bonding site of the interface Ca atom relative to the Si substrate in this study; the site shown was determined by medium-energy ion scattering.[25]

The growth morphology of CaF_2 or SrF_2 on Si(111) depends strongly on the kinetic parameters of substrate temperature, incident flux, and substrate miscut angle. For variations of these parameters, we have shown that either islanded films (e.g., Fig. 1) or flat films (i.e., with no exposed reacted layer) may be obtained.[26,27] CaF_2, in particular, has an interesting growth mode in which the minimum thickness for a well-defined two-dimensional film is three TL's. For thinner films, the initial growth mode is Stranski-Krastanov-like, in which the substrate is uniformly covered by a single Si-Ca-F interface layer, on top of which grow 2-TL-high, bulklike islands; these thin islands merge together to form a uniform film. This film becomes a template for subsequent layer-by-layer growth. If the growth rate is too slow, the substrate temperature too high, or the step density too great, then the diffusion time of CaF_2 molecules towards step edges is shortened relative to the intermolecular collision time. Under these conditions, thick islands nucleate at step edges resulting in rough films with an exposed Si-Ca-F reacted layer between the islands.[28]

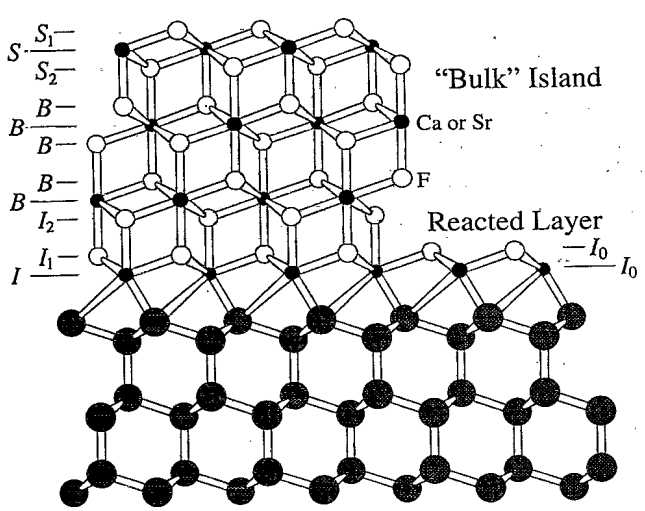

FIG. 1. Labeling convention for Ca (Sr) and F atoms in CaF_2(SrF_2) on Si, of the general case of flat islands atop a reacted Si-Ca-F (Si-Sr-F) bilayer. The exposed interface atoms are designated with a subscript zero to distinguish them from buried interface atoms.

Previously, interface core-level shifts (ICLS's) were observed for Ca, Sr, and F atoms in the interface layers.[22–24] In this study we have resolved a second F ICLS as well as the SCLS's for multilayer films using an *in situ* combination of XPS and x-ray-photoelectron diffraction (XPD). This combination enhances the resolution of XPS alone; additionally it confirms the film morphologies and atomic arrangements. Moreover, for films in which there is both an uncovered and a covered reacted interface layer (Fig. 1), we have resolved the CLS's between buried (I,I_1,I_2) and exposed (I_0) atoms as well. In addition to the XPS spectra, we have also observed shifts in AES for both Ca and F atoms. This independent measurement allows us to estimate the relative contribution of initial- and final-state terms in CaF_2 films. We separately compute these effects using the model of Rotenberg and Olmstead;[13] this model is presented in Sec. II. The experimental results are presented in Sec. III, and the interpretation of these data is given in Sec. IV, where we infer information about chemical states at the surface and interface.

Finally, we briefly review the XPD technique. In XPS,[1–3] the photoelectron energy spectrum is recorded by integrating electrons over a large angular acceptance at high-energy resolution. In XPD,[29,30] this acceptance is reduced to measure the angular distribution of elastically scattered electrons; the energy resolution is relaxed to enhance data collection efficiency. If the kinetic energies are a few hundred or more electron volts, photoelectrons are preferentially scattered along axes between the source atom and other atoms between the source and the detector, an effect called "forward focusing." If no atoms lie between the source atom and the detector, then the angular distribution of photoelectrons will be uniform (insofar as one can neglect backscattering from underlying atoms, as happens for the kinetic energies used here).

II. THEORY

A. Contributions to CLS's

We consider the photoemission process to occur in three steps. In the first, the electron is emitted from the atom, and all other electrons in the solid are frozen in their initial states. The kinetic energy of the electron is determined by the electrostatic interaction with the other charges in the system, i.e., by the initial-state potential at the core level in question. In the second step, the remaining electrons respond to the sudden appearance of the core hole by relaxing to their final-state configuration. Since this electronic relaxation occurs on the same time

scale as the photoemission process, the interaction between the photoelectron and the solid is modified, thus changing the kinetic energy, and hence the apparent binding energy of the photoelectron. In the third and final step, electrons propagate to the detector, scattering both elastically (yielding XPD modulations) and inelastically.

The total photoemission (PE) core-level shift between two atoms A and B with the same intra-atomic configuration is given by

$$\Delta E_{\mathrm{PE}}=(E_B-E_A)_{\mathrm{PE}}=e\Delta\Phi_M+\Delta R \ , \tag{1}$$

where $e\Delta\Phi_M$ is the extra-atomic initial-state shift, ΔR is the extra-atomic final-state shift, and by convention positive ΔE, $\Delta\Phi_M$, and ΔR correspond to a core-level electron more bound to (having less kinetic energy from) atom B than atom A. For Auger emission (AE), the observed reduction in kinetic energy is

$$\Delta E_{\mathrm{AE}}=(E_B-E_A)_{\mathrm{AE}}=e\Delta\Phi_M+3\Delta R \ . \tag{2}$$

This equation is verified theoretically as follows:[31,32] The final-state energy scales as the square of the core-hole charge Q. Before Auger decay, the solid has already relaxed in response to the initial core-hole charge $Q=e$; afterwards, the system responds to the final core-hole charge $2e$. Therefore the net relaxation for Auger electrons is $(2^2-1^2)\Delta R=3\Delta R$. The initial-state energy $e\Delta\Phi_M$ only scales as Q, so that the net initial-state energy shift is just $(2-1)e\Delta\Phi_M=e\Delta\Phi_M$. By measuring both ΔE_{PE} and ΔE_{AE}, we determine both ΔR and $\Delta\Phi_M$ using Eqs. (1) and (2), which may then be compared to theoretical results. Equation (2) has been established experimentally for the case $\Delta\Phi_M=0$ for the rare-gas solid Xe.[8] In this paper we apply Eq. (2) to the general case $\Delta\Phi_M\neq 0$ in CaF_2 and SrF_2. This is plausible since for fully ionized atoms, both the anion and cations have closed-shell configurations, similar to Xe. We have already outlined the calculation of ΔR and $\Delta\Phi_M$ in a previous publication;[13] further details are provided below.

B. Initial-state shift

To model thin, crystalline, insulating films, we exploit the translational symmetry in the direction parallel to the surface, and allow for any arrangement of atoms in the perpendicular direction. The direct lattice of the film is described by two-dimensional lattice vectors $\{\mathbf{R}_\parallel\}$, with a corresponding set of reciprocal space vectors $\{\mathbf{G}_\parallel\}$. The basis set for the crystal is given by the set of vectors $\{\rho_t\}$ where the position of the photoemitting atom $\rho_0=0$, and we define the z direction to be perpendicular to the film. The initial-state shift ΔE_i in these ionic films is modeled with the electrostatic (Madelung) potential

$$(\Delta E_i)/e=\Phi_M=\sum_{\mathbf{R}_\parallel}\sum_t q_t/|\mathbf{R}_\parallel+\rho_t| \tag{3}$$

at the site of the photoemitting atom due to the other ions of charge q_t at positions $\mathbf{R}_\parallel+\rho_t$ relative to the source atom. We compute this potential using the method of Parry[6] in which the standard Ewald method is modified for two-dimensional systems. In this method, the conditionally convergent summation in Eq. (3) is broken into fast-converging summations in reciprocal and direct space; it becomes

$$\begin{aligned}\Phi_M=&\sum_{\mathbf{G}_\parallel}\sum_t S_t(\eta,\mathbf{G}_\parallel)\exp(-i\mathbf{G}_\parallel\cdot\rho_{t,\parallel})\\&+\sum_{\mathbf{R}_\parallel}\sum_t q_t\mathrm{erfc}(|\mathbf{R}_\parallel+\rho_t|\sqrt{\eta})/|\mathbf{R}_\parallel+\rho_t|\\&-2q_0\sqrt{\eta/\pi}\ ,\end{aligned} \tag{4}$$

where $\rho_{t,\parallel}$ are the coordinates of the basis atoms parallel to the surface and q_0 is the charge of the ion emitting the electron. The third term in Eq. (4) is a correction that effectively excludes the core electron from the computed potential. The computed potential is independent of the parameter η, which is chosen so that the two summations converge in roughly the same number of terms (typically $\sqrt{\eta}\approx 0.5$ Å^{-1}). The structure factor S_t contains information perpendicular to the surface and is given by

$$\begin{aligned}S_t(\eta,\mathbf{G}_\parallel\neq 0)=&q_t\left[\frac{\pi}{\alpha G_\parallel}\right]\\&\times\left\{e^{-G_\parallel\rho_{t,z}}\mathrm{erfc}\left[\frac{G_\parallel-2\eta\rho_{t,z}}{2\sqrt{\eta}}\right]\right.\\&\left.+e^{G_\parallel\rho_{t,z}}\mathrm{erfc}\left[\frac{G_\parallel+2\eta\rho_{t,z}}{2\sqrt{\eta}}\right]\right\}\ ,\end{aligned} \tag{5a}$$

where α is the area of the unit cell in real space and $\rho_{t,z}$ is the position of the tth basis atom in the direction normal to the film surface. Particular attention must be paid to the case of $\mathbf{G}_\parallel=0$, in which case the first term in Eq. (4) becomes

$$\begin{aligned}\sum_t\rightarrow\frac{2\pi}{\alpha}\sum_{t\neq 0}q_t\{&(\eta\pi)^{-1/2}[1-\exp(-\eta\rho_{t,z}^2)]\\&-\rho_{t,z}\mathrm{erf}(\sqrt{\eta}\rho_{t,z})\}\ ,\end{aligned} \tag{5b}$$

where we have used the facts that the unit cell of the lattice must be charge neutral and that $\rho_0=0$. Equation (5b) is zero only in the case where the unit cell contains no net charge in any given layer perpendicular to the film.

C. Final-state shift

The relaxation shift ΔR is computed in direct space because translational symmetry is lost when the system responds to the core hole. The lattice is modeled as a finite cluster of maximum radius ρ and consists of a set of polarizable dipoles, whose configuration (angle and magnitude) in the presence of the core hole is to be calculated. The relaxation energy ΔR thus depends on the geometry and the polarizabilities α_+ and α_- of the anion and cation, respectively. The dipole configuration for a finite cluster of atoms is given self-consistently by the matrix equation[11,33]

$$\mathbf{p}^i=\alpha_i\mathbf{E}^i_{\text{loc}}=\alpha_i\mathbf{E}^i_{\text{fixed}}+\sum_{j\neq i}\mathbf{M}^{ij}\cdot\mathbf{p}^j\ , \tag{6}$$

where $\mathbf{p}^i$ is the ith dipole moment, $\mathbf{E}^i_{\text{loc}}$ is the local field at the ith dipole, $\mathbf{E}^i_{\text{fixed}}$ is the fixed field $\mathbf{E}_0=Q\mathbf{r}/r^3$ from the core hole, plus any other fixed fields (see below). The matrix $\mathbf{M}^{ij}$ encodes the locations and polarizabilities of the dipoles; its components are given by

$$M^{ij}_{kl}=\alpha_j(3R^{ij}_kR^{ij}_l|\mathbf{R}^{ij}|^{-5}-|\mathbf{R}^{ij}|^{-3})\ , \tag{7}$$

where $\mathbf{R}^{ij}=(\mathbf{R}^i-\mathbf{R}^j)$ is the vector from the jth dipole to the ith dipole; k and l denote Cartesian coordinates. The size of the matrix in Eqs. (6) and (7) may be greatly reduced by grouping together similar dipoles whose orientations are related by symmetry.[33] Once Eq. (6) is inverted, the total relaxation energy of the cluster is computed from the expression

$$R_{r<\rho}=-\tfrac{1}{2}\sum_i\mathbf{E}_0\cdot\mathbf{p}_i\ . \tag{8}$$

It is not practical to choose a large enough cluster for Eq. (8) to converge as $\rho\to\infty$. Therefore, the relaxation energy of dipoles outside the cluster is estimated from the continuum expression

$$R_{r>\rho}=-\tfrac{1}{2}\int\mathbf{E}_0\cdot\mathbf{P}\,dV \tag{9}$$

(where $\mathbf{P}$ is the continuum polarizability), so that the total relaxation R is given by the sum of Eqs. (8) and (9). For bulk, surface, and thin-film geometries, Eq. (9) becomes

$$R^{\text{bulk}}_{r>\rho}=-\frac{1}{2}\left[1-\frac{1}{\varepsilon_\infty}\right]\frac{Q^2}{\rho}\ , \tag{10a}$$

$$R^{\text{surf}}_{r>\rho}=R^{\text{bulk}}_{r>\rho}\left[\left[\frac{1}{2}+\frac{d_s}{4\rho}\right]+\frac{Q'}{Q}\left[\frac{1}{2}-\frac{d_s}{4\rho}\right]\right]\ , \tag{10b}$$

$$R^{\text{film}}_{r>\rho}=R^{\text{bulk}}_{r>\rho}\left[\left[\frac{d_i+d_s}{4\rho^2}\right]+\sum_{n=1}^{\infty}\frac{Q_n}{2Q}[f_1(n)+f_2(n)+f_3(n)+f_4(n)]\right]\ , \tag{10c}$$

where

$$f_1(n)=-0.5(2d_i+d_n)^{-1}\ , \tag{10d}$$

$$f_2(n)=0.5(-2d_s+d_n)^{-1}\ , \tag{10e}$$

$$f_3(n)=\frac{(d_i+d_n)[2d_id_n+d_n^2+\rho^2]^{1/2}}{(2d_i+d_n)(d_n\rho)}\ , \tag{10f}$$

$$f_4(n)=\{(\rho^2-d_n^2)[-2d_sd_n+d_n^2+\rho^2]^{1/2}-[-2d_sd_n+d_n^2+\rho^2]^{3/2}\}/(-2d_s+d_n)(2d_n^2\rho)\ , \tag{10g}$$

and $d_s,d_i<\rho$ are the distances from the core hole to the surface and interface, respectively. Equations (10b) and (10c) derive from the interaction of the far region $r>\rho$ (with dielectric constant ε_∞) and either a single-image charge

$$Q'=Q(\varepsilon_\infty-1)/(\varepsilon_\infty+1) \tag{10h}$$

or an infinite series of charges, with positions d_n (relative to the core hole) and charges Q_n given by[34]

$$d_n=n(d_i+d_s)+0.5(d_i-d_s)[(-1)^n-1]\ , \tag{10i}$$

$$Q_n=Q\times\begin{cases}\xi^{|n|/2}\ , & n\ \text{even}\\ \xi^{(n-1)/2}\dfrac{\varepsilon_{\text{film}}-\varepsilon_{\text{vac}}}{\varepsilon_{\text{film}}+\varepsilon_{\text{vac}}}\ , & n\ \text{odd}\ ,\ n>0\\ \xi^{(-n-1)/2}\dfrac{\varepsilon_{\text{film}}-\varepsilon_{\text{sub}}}{\varepsilon_{\text{film}}+\varepsilon_{\text{sub}}}\ , & n\ \text{odd}\ ,\ n<0\ ,\end{cases} \tag{10j}$$

where

$$\xi=\frac{\varepsilon_{\text{film}}-\varepsilon_{\text{sub}}}{\varepsilon_{\text{film}}+\varepsilon_{\text{sub}}}\frac{\varepsilon_{\text{film}}-\varepsilon_{\text{vac}}}{\varepsilon_{\text{film}}+\varepsilon_{\text{vac}}}\ . \tag{10k}$$

Because of the short time scale of the emission process (<1 fs), the substrate and film dielectric constants (ε_{sub}, $\varepsilon_{\text{film}}$) are taken in the limit of large frequency ($\omega\to\infty$). This limit implies no distortion of the ionic lattice in response to the core hole.

To ensure continuity of the polarization across the boundary $r=\rho$, a small correction of Eq. (6) may be made.[35] The local fields at dipoles near $r=\rho$ contribute an additional term to $\mathbf{E}^i_{\text{fixed}}$ in Eq. (6); however, calculations of this correction showed it to be less than 0.5% of R for sufficiently large clusters, so it is neglected for the results given below. For films and surfaces, the residual continuum expression in Eq. (9) necessarily includes arbitrary parameters—the exact position of the surface and interface relative to the cluster atoms. The cluster part of the calculation, which dominates the total relaxation energy, contains no such parameters. Therefore, for sufficiently large clusters, the calculation is not very sensitive to these parameters, resulting only in an additional uncertainty of $\sim$0.5% in the total relaxation energies.

Figure 2 illustrates the calculation of $e\Delta\Phi_M$ and ΔR for the Ca and F atoms near the CaF_2 (111) surface for a cubic, semi-infinite solid at its natural lattice constant. The total Auger and photoelectron shifts [Figs. 2(a) and 2(b)] are computed from Eqs. (2) and (1), respectively. The only parameters in the calculation are the polarizabilities[36] of Ca and F atoms, $\alpha_+=0.979$ Å^3 and $\alpha_-=0.759$ Å^3, respectively. The calculated data (open symbols) indicate the computed relaxation shift ΔR; the dashed lines indicate the best fit to the function

$$\Delta R(z)=-Q^2(\varepsilon_\infty-1)/[4\varepsilon_\infty(\varepsilon_\infty+1)(z-z_0)]\ , \tag{11}$$

which, for $z_0=0$, is the same as predicted for a point charge in a continuous semi-infinite dielectric. This expression is derived from the interaction of the core hole and its image charge across the surface; the binding energy is enhanced near the surface because the vacuum is not polarizable whereas CaF_2 is. Hence core holes near the surface induce less polarization than those within the

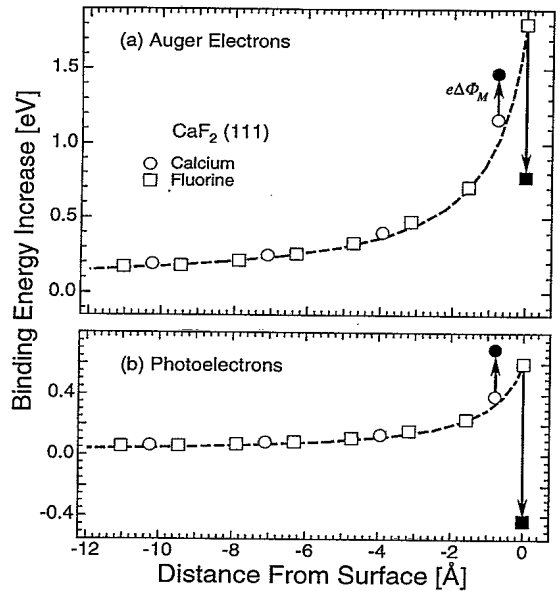

FIG. 2. Theoretical calculation of (a) surface Auger shifts $\Delta E = e\Delta\Phi_M + 3\Delta R$ and (b) surface core-level shifts $\Delta E = e\Delta\Phi_M + \Delta R$ for a CaF_2 (111) surface. The open symbols are the relaxation term only, and the closed symbols are the relaxation plus Madelung terms. The dashed lines represents a simplified image-charge approximation to the relaxation term (see text). The arrows indicate the Madelung term, which is significant only for the two surface atoms shown.

bulk. The parameter z_0 specifies an effective position of the surface relative to the nuclei of the surface atoms. We find the best agreement for $z_0 \sim 1.0$ Å above the surface F nucleus, which is close to the ionic radius of F^-. A similar relationship was also found to hold for NaCl(100) and Xe(111).[13] The agreement between the dashed lines and the computed points indicates the validity of the image-charge approximation even within a lattice constant of the surface.

The calculated Madelung shifts $\Delta\Phi_M$ are indicated in Fig. 2 by the arrows; the shifts are completely negligible (≤ 0.015 eV) except for the near-surface atoms indicated. As is generally true for ionic crystals, $e\Delta\Phi_M$ adds (subtracts) from the Ca (F) surface binding energy shift predicted from ΔR alone.

D. Substrate effects

There are three substrate effects which we consider in this paper. The first effect is the chemical (intra-atomic) contribution to the ICLS, which is due to the bond between interface Ca and Si. While calculation of this effect is beyond the scope of this paper, its magnitude may be estimated from the difference between the experimental values and the calculated extra-atomic effects. This will be discussed further in Sec. IV A. The second effect is the distortion of the film due to strain from lattice mismatch. This effect is most important for SrF_2 on Si(111) and its inclusion in the calculation is discussed in Sec. IV B. The third effect is the polarizability of the substrate, which affects both the Madelung and relaxation energies. This is considered in the remainder of this section.

In the initial state, the substrate polarizes (through lattice and bonding orbital distortion) due to the electrostatic fields of the overlayer ions. The potential at each overlayer ion is in turn altered by this polarization field. This potential may be approximated by the potential of an inverted, "image lattice" composed of image charges of the ionic lattice reflected across the insulator-substrate interface.[37] This effect, however, turns out to be negligible for all but the Ca or Sr atoms at the substrate interface due to the strong exponential attenuation of the Madelung potential and the large distance between the real and image lattices. But even for the interface atoms, the effect is small ($<25\%$ of $e\Delta\Phi_M$ at the interface) and is neglected.

The substrate has a much stronger effect on the final-state energy for interface emission. The substrate polarizes dynamically in response to the core hole, and, for metallic or semiconducting substrates (which have high dielectric strength), the substrate polarization dominates the observed interface core-level shifts. We cannot apply the simple point-polarizable atomic model to these substrates because the polarizable units are not localized to atomic sites, but are diffused throughout the crystal as free electrons or as covalent bonds. Instead, to include the substrate's relaxation, we have modified Eq. (6) as follows: (i) each dipole $\mathbf{p}^i$ in the cluster undergoes an additional field due to an "image" core hole of strength $Q' = -Q\ (\varepsilon_{sub}-1)/(\varepsilon_{sub}+1)$ and distance $2d_i$ from the "real" core hole, and (ii) each $\mathbf{p}^i$ feels the additional fields of an array of "image" dipole reflected across the interface with a continuum dielectric. The orientation of the image dipoles relative to the real dipoles is inverted in the plane parallel to the interface, while the magnitude is reduced by the factor $|Q'/Q|$. Finally, to account for the substrate's polarization response, the total relaxation energy becomes $R = R_{r<\rho} + R_{r>\rho} + QQ'/4d_i^2$.

This procedure introduces a new parameter to the calculation of Eqs. (6)–(9): the exact position d_i of the interface relative to the core hole. While $R_{r>\rho}$ is not sensitive to this position (for sufficiently large clusters), $R_{r<\rho}$ is very sensitive to it [Eq. (8)]. For thin films, we allow this parameter to vary to find the best match to experiment, and the best-fit position for CaF_2 was 0.8 Å from the center of the interface Ca atoms, which is within the Ca-Si bond.

III. EXPERIMENTAL CLS's

In this section, we detail the experimental measurements of the CLS's in CaF_2 and SrF_2 films on Si(111). The resulting shifts and comparison with theoretical calculations are presented in Tables I and II for CaF_2 and SrF_2, respectively. Section IV will discuss the results and compare them to theory.

A. Growth conditions

CaF_2 and SrF_2 were deposited from separate graphite crucibles onto resistively heated, p-type ($\approx 1\ \Omega$ cm), on-axis (miscut $<0.25°$) Si(111) wafers in an ultrahigh vacu-

TABLE I. Summary of CaF_2 CLS's for various geometries. Experimental and theoretical values are reported in eV, where positive shifts correspond to higher binding energy (lower kinetic energy) than the bulk reference peak.

Geometry	Atom	Photoelectrons Theory	Photoelectrons Expt.	Auger electrons Theory	Auger electrons Expt.
8-TL film	F (S_1)	−0.54		0.54	0.53±0.1
	Ca (S)	0.64	0.63±0.13	1.32	
	F (S_2)	0.16		0.50	0.53±0.1[a]
4-TL film	F (S_1)[b]	−0.45		0.75	0.7±0.2
	Ca (S)[b]	0.74	0.71±0.09	1.61	1.2±0.4
	F (S_2)[b]	0.20		0.63	0.7±0.2[a]
	F (I_2)[b]	−0.33		−0.99	1.5±0.5
	F (I_1)[b]	−0.98		−2.92	−3.04±0.03
	Ca (I)[b]	−2.05	−2.65±0.05	−6.78	−5.05±0.5
3-TL film	F (S_1)[b]	−0.46		0.71	0.51±0.05
	Ca (S)[b]	0.75	0.63±0.1	1.63	1.5±0.5
	F (S_2)[b]	0.16		0.50	0.51±0.05[a]
	F (I_2)[b]	−0.25	−0.35±0.1	−0.75	−1.1±0.3
	F (I_1)[b]	−0.92	−0.75±0.1	−2.72	−2.74±0.04
	Ca (I)[b]	−1.96	−2.42±0.05	−6.51	−4.3±0.5
3-TL film	F (S_1)[c]		−0.35±0.35		−2.4±0.1
+ oxygen	Ca (S)[c]		−2.0±0.1		−3.9±0.5
Islands	F (I_0)[d]	−0.55	−1.30±0.2	0.54	−0.84±0.3
with exposed interface	Ca (I_0)[d]	0.64	0.20±0.05[e]	1.32	≥0

[a]Not resolved from S_1.
[b]Shifts relative to remaining bulk atoms.
[c]Shifts relative to uncovered surface atoms.
[d]Shifts relative to buried interface atoms F (I_1) and Ca (I).
[e]Data averaged over four samples.

um chamber. Unless otherwise indicated, the substrate temperatures were 700 °C and the incident flux was 50 Å/min, calibrated with a quartz-crystal oscillator. The base pressure was below 10^{-10} Torr, and the growth pressure was typically 10^{-8} Torr, mainly consisting of N_2 outgassed from BN insulators in the growth cells. The substrates were prepared using either Shiraki etching and annealing, or repeated sputter-anneal cycles, until the substrates exhibited sharp 7×7 low-energy electron-diffraction (LEED) patterns, Si 2p energy and line shape characteristic of (111)7×7 surfaces, and no measurable oxygen XPS signal. The sample temperature was measured by an optical pyrometer and is expected to be relatively accurate to within a few degrees; according to our calibration, the Si substrate 7×7→1×1 transition temperature was observed with LEED to occur at ~835 °C. After the samples were grown, electron spectra were acquired without removing the samples from ultrahigh vacuum. Once a film was grown, LEED was not performed until all spectra were acquired; this was to avoid damaging the films by electron-beam exposure.

We also allowed some samples to remain exposed to the residual gases of our chamber for several days. The only adsorbed contaminant we observed was several chemically distinct species of adsorbed oxygen. These species have different desorption energies as determined by annealing studies and may be due to first- and higher-contaminant layers. The appearance of these species, discussed further elsewhere,[38] are correlated with our Ca and F observations to confirm our assignments of Ca and F surface atoms.

XPS spectra were acquired with Mg K_α illumination

TABLE II. Summary of SrF_2 SCLS's. Experimental and theoretical values are reported in eV, where positive shifts correspond to higher in binding energy (lower kinetic energy) than the bulk reference peak.

Geometry	Atom	Photoelectrons Theory	Photoelectrons Expt.	Auger electrons Theory	Auger electrons Expt.
Islands	F (S_1)	−0.58		0.45	0.64±0.08
with exposed	Sr (S)	0.64	0.63±0.08		
interface	F (S_2)	0.14		0.46	0.64±0.08[a]

[a]Not resolved from S_1.

($h\nu = 1253.6$ eV). Spectra were mathematically deconvolved using a Fourier-transform technique to remove satellite $K\alpha'$ and $K\alpha_{3,4}$ x-ray lines. This was the only deconvolution used before fitting the spectra. For display purposes, a similar deconvolution was performed to remove high-frequency noise and to deconvolve the Ca $2p_{1/2}$ and Sr $3d_{3/2}$ spin-orbit-split replicas, using splittings and ratios determined from thick films.[39] Background subtraction in all cases was restricted to a constant offset fit to the low binding-energy side of our spectra; the background shape was incorporated into our fitting line shapes. The electron spectrometer used was a 126-mm hemispherical analyzer (Leybold EA-11), with a fixed angle between the x-ray source and the electronic analyzer of 55°. All binding energies are reported relative to the Fermi level E_F, which was calibrated by measuring the binding energy of Au $4f_{7/2}$ electrons (-84.0 eV below E_F). For XPS spectra, the angular acceptance cone was approximately 10°; to acquire XPD data, this acceptance was reduced to $\sim 4°$ by altering the input lends voltages. The sample holder rotates both in the polar angle θ and azimuthal angle ϕ, where $\theta = 0$ means electron emission is normal to the sample surface. Full $-90°$ to $+90°$ polar spectra were taken in the $[\bar{1}10]$ plane in two separate scans from $-90°$ to 0° at azimuthal angles of $\phi = 0°$ (towards substrate $[\bar{1}\bar{1}2]$) and $\phi = -60°$ (towards substrate $[\bar{2}11]$). Because the overlayer has type-B orientation (rotated 180° about [111]), these direction indices are inverted relative to the overlayer's indices. For each angle in a scan, a complete XPS or Auger spectrum is taken and stored for later automated curve fitting. Further details of the XPD apparatus used here are published elsewhere.[26]

We have measured the surface and interface core-level shifts for CaF_2 (Ca $2p$, F $1s$, Ca *LMM*, and F *KVV*) and SrF_2 (Sr $3d$, F $1s$, and F *KVV*) films. Below, we describe the technique for determining these shifts in detail for the Ca $2p$ electrons, and then given the results for the other peaks. Tables I and II summarize the observed CLS's for CaF_2 and SrF_2, respectively.

B. CaF_2 SCLS's

Typical XPS and XPD results are shown in Fig. 3 for a four-layer CaF_2 film consisting of a reacted Si-Ca-F bilayer at the interface and three F-Ca-F triple layers. We show in Fig. 3(a) Ca $2p_{3/2}$ core-level spectra $\mathcal{S}_{on}$ obtained at "on-axis" emission angle $\theta = 0°$, $\mathcal{S}_{off}$ at "off-axis" emission angle $(\theta,\phi) = (-26°, -18°)$, and the resulting difference spectrum $\mathcal{S}_{on\text{-}off}$. We measured the emission over the full sector $-60° < \phi < 0°$ and found that emission at the off-axis angle chosen approximates the isotropic emission amplitude in the absence of all elastic scattering.[40]

The coarse features in the spectra in Fig. 3(a) are two peaks of separation ~ 2.7 eV. The smaller-intensity peak I to lower binding energy has previously been identified as emission from the interface Ca atom bonded to the Si substrate,[22,23] while the remaining peak $S+B$ is further resolved using the method discussed below into two closely spaced components due to surface (S) and bulk-like (B) atoms.

We illustrate the effect of forward focusing in Fig. 3(b), in which I and $S+B$ XPD scans are presented as a function of θ in the plane formed by the on and off axes ($\phi = -18°$). These data were obtained by repeatedly acquiring spectra similar to those in Fig. 3(a) at each angle, performing a least-squares fit to two components, and storing the peak heights. Both scans exhibit a strong forward-scattering feature at $\theta = 0°$ (on axis) compared to the emission level observed near $\theta = 26°$ (off axis).

This forward-scattering effect is exploited to resolve the $S+B$ peak into separate surface and bulk components. Since atoms with a uniform angular distribution must contribute equally to both on- and off-axis spectra, the difference spectrum in Fig. 3(a) reflects emission only from those atoms that have scattering centers located directly above them in the [111] direction. In the difference spectrum, it is evident that the Ca peak labeled $S+B$ has narrowed and its center has shifted towards lower binding energy. Furthermore, the new, narrower width is comparable to the width for the interface signal,

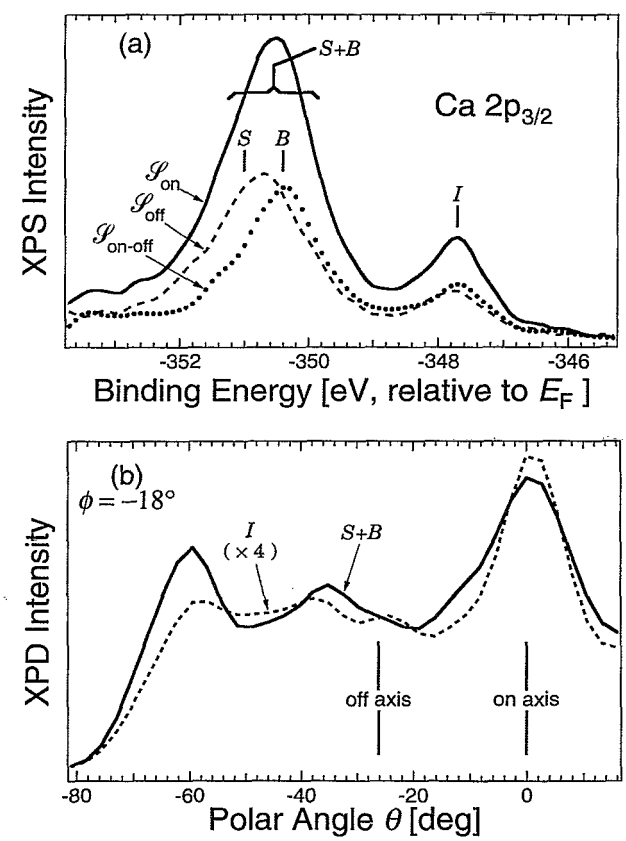

FIG. 3. XPS and XPD results for a 4-TL CaF_2/Si(111) film. (a) Ca $2p_{3/2}$ core-level spectra $\mathcal{S}_{on}$ acquired at on-axis emission ($\theta = 0°$, solid), $\mathcal{S}_{off}$ acquired at off-axis emission ($\theta = -26°$, $\phi = -18°$, dashed), and the difference spectrum $\mathcal{S}_{on\text{-}off}$ (dotted). The assignment of the surface S, bulk B, and interface I peaks is indicated by the vertical lines. (b) XPD profiles taken in the $\phi = -18°$ plane, showing the interface (dashed) and combined surface plus bulk (solid) peak heights as a function of emission angle θ. The on- and off-axis angles are indicated by vertical lines.

in which only one Ca component can be resolved. These observations can only be explained by having subtracted an unmodulated peak S at higher binding energy, which we assign to be the surface-shifted Ca contribution. The two bulklike layers of Ca between the surface and interface layers contribute a single unresolved peak B to the difference spectrum (see Fig. 1).

To quantify the S-B splitting, it is necessary to curve fit the spectra in Fig. 3(a). In XPS analysis, spectra are typically fitted with analytic functions (such as Gaussian-convolved Lorentzians) to describe the energies, heights, and widths of peaks. In this study, however, we found more satisfactory results by using empirical line shapes for interface and overlying atoms. This was because of the presence of inelastic scattering, which alters the interface line shape from the simple analytical forms. In addition, for the Auger-electron spectra to be discussed later, no simple functions exist to account for the complicated multiplet line shapes.

For the Ca atoms at the interface, we take as our interface line shape the spectrum of a single bilayer of Ca-F deposited on Si(111). For the other Ca atoms, we have taken as our line shape the spectrum from a very thick ($\sim$700 Å) sample in which only a single sharp peak predominates. The interface line shape used is an average of four different Ca-F ML samples grown under identical conditions of 5 Å/min and substrate temperature of 750 °C; it contains a satellite peak of magnitude $\sim$25% compared to the main line shape, located $\sim$4.5 eV to higher binding energy. The satellite was apparent in each of the four individual ML spectra, and is seen in all the samples in this paper (an equivalent feature is also observed in SrF_2/Si samples). The origin of this satellite is discussed elsewhere.[41,42]

Mathematically, the fitting problem may be described as follows: the off axis, on axis, and different spectra, $\mathcal{S}_{\text{off}}$, $\mathcal{S}_{\text{on}}$, and $\mathcal{S}_{\text{on-off}}$ may be written as

$$\mathcal{S}_{\text{off}}=S+B+I\ , \tag{12a}$$

$$\mathcal{S}_{\text{on}}=S+(1+\beta)B+(1+\iota)I\ , \tag{12b}$$

$$\mathcal{S}_{\text{on-off}}=\beta B+\iota I\ , \tag{12c}$$

where S, B, I are the off-axis (approximately average) signals from the surface, bulklike, and interface atoms, and β and ι are the forward focusing enhancements in the [111] direction for the bulklike and interface atoms. Because of multiple and inelastic scattering, the enhancements β and ι depend on the precise arrangement of overlying atoms, and are usually only approximately equal. From Fig. 3(b) and data from other samples we observe $\iota\approx\beta\approx1.1$ for the Ca $2p$ emission, so that we have considered the linear combination of $\mathcal{S}_{\text{on}}$ and $\mathcal{S}_{\text{off}}$, defined as

$$\mathcal{S}^*\equiv(1+\iota)\mathcal{S}_{\text{off}}-\mathcal{S}_{\text{on}}=\iota S+(\iota-\beta)B \approx\iota S\ . \tag{12d}$$

This combination is useful because for thin enough films (where B is not too large) the term ιS dominates $\mathcal{S}^*$.

Figure 4 illustrates our fitting procedure. First we fit the difference spectrum $\mathcal{S}_{\text{on-off}}$ to locate the core-level energies of the interface and buried atoms using a least-squares method [Fig. 4(a)]. The energy difference between bulk and interface emission can usually be estimated in this procedure to within $\sim\pm0.05$ eV. Having fixed the positions of the interface and bulk peaks, we use them to obtain un upper and lower limit to the bulk-surface splitting. For the upper limit, we construct the spectrum $\mathcal{S}^*$ using the smallest value of ι consistent with the data in Fig. 3 and fit it with a single bulklike component (as ι increases, the contribution of B to $\mathcal{S}^*$ shifts the apparent position of S towards B). To get a lower limit on the splitting, we simultaneously fit the $\mathcal{S}_{\text{on}}$ and $\mathcal{S}_{\text{off}}$ spectra to three peaks S, B, and I where the positions of B and I are fixed to the known positions from analysis of $\mathcal{S}_{\text{on-off}}$. When fitting peaks under these conditions, the fitting algorithm used always underestimates the S/B splitting and overestimates the S/B height ratio, thus giving us a lower limit to the surface-bulk splitting. Using this procedure, we determine the Ca surface-bulk energy shift to be 0.71 ± 0.09 eV and the bulk-interface shift to be 2.65 ± 0.05 eV. The SCLS (S relative to B) is observed to be the same from films 3–8 layers thick within the experimental uncertainties; the ICLS (I relative to B) was found to be somewhat variable from growth to growth and was especially sensitive to the growth temperature;[22–24,42] furthermore, the splitting sometimes widened slightly (with the interface position remaining fixed) in the first hour after growth. All of the spectra discussed in this paper were acquired after this widening (if any) was complete.

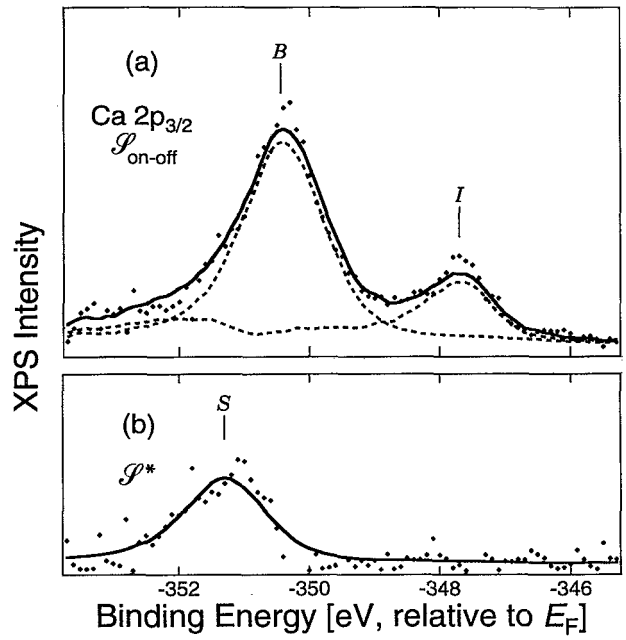

FIG. 4. Curve fits for the 4-TL CaF_2 film in Fig. 3. (a) Difference spectrum $\mathcal{S}_{\text{on-off}}$, which is only sensitive to bulk and interface Ca atoms. (b) Linear combination $\mathcal{S}^*=2.1\mathcal{S}_{\text{off}}-\mathcal{S}_{\text{on}}$, which is primarily sensitive to surface Ca atoms.

Close examination of Fig. 4(a) shows that the Ca line shape from the unburied interface used in the fit is some-

what broader than the actual signal from the buried interface Ca atoms; an even larger width difference is observed for interface F atoms. This suggests that there is some disorder in the position of the F atoms in the bare Si-Ca-F layer and that these F atoms are ordered upon being covered. This is supported by the fact that at low coverages, the XPD forward focusing of Ca photoelectrons by F atoms in the $[11\bar{1}]$ direction is reduced from the expected magnitude obtained from theoretical modeling, as well as compared to surface Ca→F $[11\bar{1}]$ forward scattering.

The atomic structures near the Ca *S*, *B*, and *I* atoms were observed for a 3-TL film (grown at 52 Å/min at 700 °C) with component-resolved XPD (CR-XPD). The separate diffraction patterns for a three-layer film are shown in Fig. 5 (dots). These curves were obtained by recording a Ca 2*p* spectrum $\mathcal{S}_\theta$ for each polar angle θ and fitting it with three peaks whose energies are fixed from prior fits to $\mathcal{S}_{\rm on}$ and $\mathcal{S}_{\rm off}$ XPS spectra. The normalized peak amplitudes are then reported in Fig. 5. There are three important facts established from this data. First, we confirm the assignment of the *S* component as the surface Ca atom. This is because while the *S* component has little modulation near $\theta=0°$, it shows significant forward scattering in the $[11\bar{1}]$ and $[\bar{1}\bar{1}3]$ directions, which would be expected for Ca→F scattering (see upper inset). This rules out the possibility that *S* results from randomly located Ca atoms, since such atoms have isotropic emission in all directions, not just near $\theta=0°$. Second, we verify the simple structural model illustrated in the insets, since theoretical single-scattering spherical-wave calculations (solid lines) agree with the XPD profiles indicated. (Recently, it was proposed[44] that the buried Si-Ca-F interface layer undergoes a strain-driven reconstruction to a $\sqrt{3}\times\sqrt{3}$ structure, which would have dramatically different XPD behavior. Our results for films at least eight TL's thick contradict this proposed interface structure.) Third, we confirm the film thickness as not being more than three TL's thick (Si-Ca-F plus two bulk TL's). This is because of the presence of the [112] scattering from second-layer atoms in the interface XPD profile and the absence of this scattering peak for the bulklike atom *B*.

Figure 6 illustrates the results for Ca $L_{23}M_{23}M_{23}$ Auger electrons for the same 4-TL film used for Figs. 3 and 4. Spectra (a)–(d) show the on-axis data $\mathcal{S}_{\rm on}$, the off-axis data $\mathcal{S}_{\rm off}$, and the linear combinations $\mathcal{S}_{\rm on\text{-}off}$ and $\mathcal{S}^*=1.95\mathcal{S}_{\rm off}-\mathcal{S}_{\rm on}$. The smaller value of $\iota=0.95$ com-

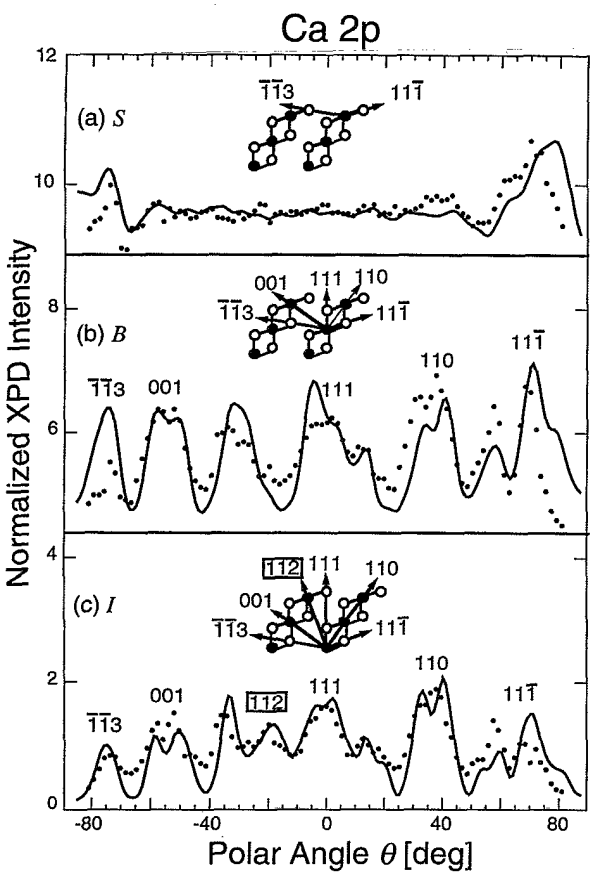

FIG. 5. Component-resolved XPD profiles (solid lines, theoretical; dots, experimental) for Ca 2*p* electrons in a 3-TL CaF_2 on Si(111) film. (a) Surface Ca atoms *S*, (b) bulklike Ca atoms *B*, (c) interface Ca atoms *I*. The insets show the corresponding in-plane scattering angles responsible for the forward-scattering peaks in the XPD profiles.

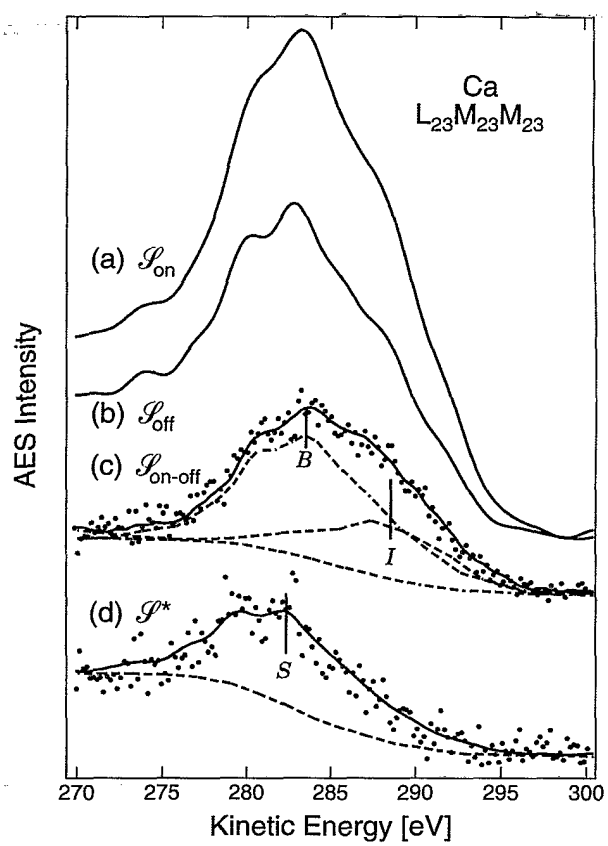

FIG. 6. Ca *LMM* AES spectra for a 4-TL CaF_2/Si(111) film. (a) Smoothed on-axis emission ($\theta=\phi=0°$), (b) smoothed off-axis emission ($\theta=-26.1°$, $\phi=-18°$), (c) raw difference spectrum $\mathcal{S}_{\rm on\text{-}off}$, which is sensitive to bulk and interface Ca atoms, and (d) raw spectrum $\mathcal{S}^*=1.95\mathcal{S}_{\rm off}-\mathcal{S}_{\rm on}$, which is sensitive to surface Ca atoms.

pared to that for Ca $2p$ is due to the reduced forward scattering at lower kinetic energy ($\sim$280 vs $\sim$900 eV). The fit to the interface and bulk core levels is indicated in Fig. 6(c), using appropriate line shapes obtained from ML and thick films. For Ca *LMM* electrons, the situation is complicated by the extremely wide ($\sim$10 eV) multiplet line shape, as well as the large inelastic-scattering background, which is different for each of the components. To compensate for the inelastic background, we subtracted the background using the Shirley method both from the spectra to be fit as well as from the empirical line shapes. After fitting, the inelastic backgrounds were restored to the spectra $\mathcal{S}$. The ICLS was found to be -5.0 ± 0.5 eV, while the SCLS was 1.2 ± 0.3 eV.

Figure 7 shows AES results for F *KVV* Auger electrons for the 4-TL film. Figure 7(a) shows the $\mathcal{S}_{on}$, $\mathcal{S}_{off}$, $\mathcal{S}_{on\text{-}off}$, and $\mathcal{S}^*=3.5\mathcal{S}_{off}-\mathcal{S}_{on}$ spectra, while Fig. 7(b) shows final fitting results. Examination of $\mathcal{S}_{on}$, $\mathcal{S}_{off}$, and $\mathcal{S}_{on\text{-}off}$ clearly indicates surface S, bulklike B, and interface I_1 fluorine atoms (as defined in Fig. 1). The feature S is comprised of two unresolved peaks S_1 and S_2 from the two fluorine atoms in the surface TL. We also observe an additional

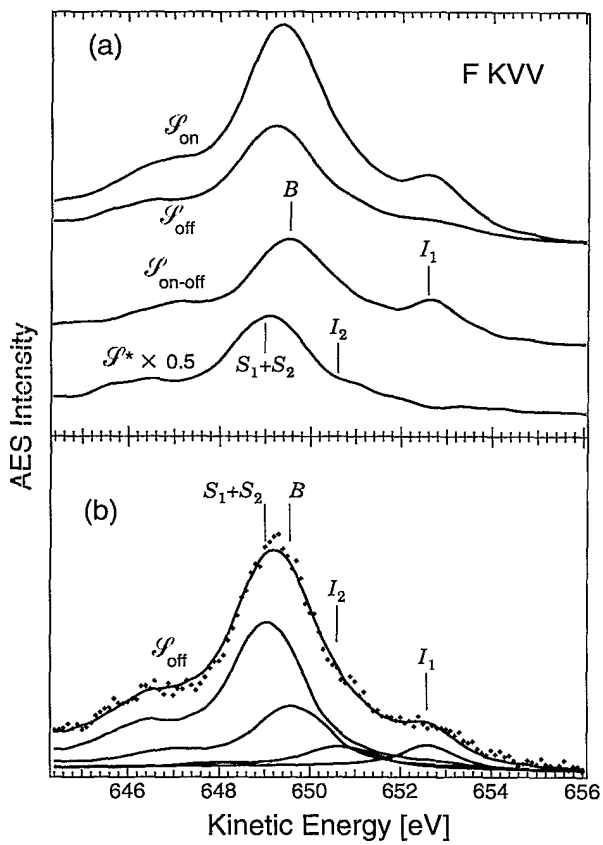

FIG. 7. F *KVV* AES results for a 4-TL CaF_2/Si(111) film. F *KVV* Auger spectra for (a) on-axis emission $\mathcal{S}_{on}$ ($\theta=0°$), off-axis emission $\mathcal{S}_{off}$ ($\theta=-26°$, $\phi=-18°$), the difference spectrum $\mathcal{S}_{on\text{-}off}$, which is sensitive to bulk and surface F atoms, and the spectrum $\mathcal{S}^*=3.5\mathcal{S}_{off}-\mathcal{S}_{on}$, which is sensitive to fluorine atoms without scattering centers in the on-axis direction. (b) The final fit to the raw $\mathcal{S}_{off}$ spectrum, showing all four components (surface atoms S_1+S_2, bulk B, and interface I_1 and I_2).

ICLS component (I_2) between B and I_1, whose existence is inferred by a combination of AES and Auger-electron diffraction (AED) as discussed below.

Analysis of fluorine data is complicated by the fact that, unlike Ca atoms, fluorine atoms have two unique sites relative to the surface normal. The upper site of a TL has a first-near-neighbor Ca atom along [111] and thus its emission is strongly focused in this direction. The lower site of a TL has a fifth-near-neighbor fluorine atom along [111] and hence its emission has negligible forward focusing in this direction (since the forward focusing amplitude is proportional to the inverse spacing between emitter and scatterer atoms[30]). Because of this, the electrons emitted from interface atoms I_1 have a much stronger forward-scattering amplitude than those emitted from bulk atoms B, which, in this 4-TL film, are an average of one weakly scattered and two strongly scattered components. This means that for fluorine atoms, β is considerably less than ι (from Fig. 7, we estimate $\beta\approx1.1$ and $\iota\approx2.5$). This affects the appearance of both the $\mathcal{S}_{on\text{-}off}$ and $\mathcal{S}^*$ spectra as follows: $\mathcal{S}_{on\text{-}off}$ has a reduced B component because one of the bulk atoms has no Ca atom directly above it. This only affects the relative amplitudes of B and I, and not the fitted energies. This unmodulated component instead appears in the $\mathcal{S}^*$ spectrum, distorting the S_1+S_2 peak. Moreover, the $\mathcal{S}^*$ spectrum displays extra intensity between I_1 and B. We assign this intensity to a second interface peak I_2, which, being of the second type of site, also has negligible forward scattering in the [111] direction. We have taken special care to verify the existence and nature of this peak, as will be discussed below.

The final off-axis fluorine *KVV* fit is shown in Fig. 7(b). The (S_1+S_2) CLS, I_2 CLS, and I_1 CLS were found to be 0.7 ± 0.2, -1.5 ± 0.5, and -3.04 ± 0.03 eV, respectively. The I_1 component sharpens considerably upon being buried; as discussed above, this is evidence for some fluorine disorder in the unexposed Si-Ca-F layer, which is removed upon further growth. Consequently, the exposed interface F line shape gave unsatisfactory fits to the data. However, use of the bulk line shape for I_1 also gave unsatisfactory fits due to differences in inelastic-scattering tails. Because of this, the interface line shape in Fig. 7(b) was derived self-consistently from a series of $\mathcal{S}_{on\text{-}off}$ from various films.

The I_2 CLS is difficult to determine from the data presented since this peak has no forward scattering in the [111] direction and hence does not appear in $\mathcal{S}_{on\text{-}off}$. The most accurate measurement of its energy is from a 3-TL film (discussed below), in which this peak was highlighted using the XPD effect. The line shape of I_2 appears to be bulklike, which is not surprising since this atom is fully coordinated.

An alternate interpretation of our data is that the I_2 component is located between the interface Si and Ca atoms. Such excess interfacial fluorine has previously been inferred from a Si $2p$ ICLS to higher binding energy, attributed to Si-F bonding.[22,23] We reject this interpretation for the following reasons: (i) In films grown under similar conditions to the ones discussed in this paper, we

have not observed evidence of a Si-F ICLS using photoemission excited by synchrotron radiation ($h\nu = 135$ eV). (ii) The I_2 component is absent from single-layer films that we have grown. (iii) The direction and magnitude of this component's energy shift relative to bulk is consistent with our theoretical calculation for the site labeled I_2 in Fig. 1. For I_2 in the alternate site (closer to the polarizable substrate), we would have a much larger core-level shift than we observe.

Similar to Ca 2*p*, we were able to confirm the F *KVV* assignments and thickness using CR-AED as shown in Fig. 8 (same 3-TL film as used for Fig. 5). The peak positions of I_1, I_2, B, and S were first determined as above (the values are summarized in Table I) and these energies were then used for fitting the CR-AED data. As mentioned above, there are two inequivalent F sites with respect to the [111] direction. I_1 and B are of the first type, which has a first-near-neighbor Ca in the [111] direction and hence strong scattering into $\theta = 0°$; I_2 is of the second type and therefore should have weak scattering into this direction. The CR-AED verifies this; in addition other scattering angles that distinguish I_1 and I_2 are indicated in the figure. Finally, the assignment of the unresolved surface atoms S is confirmed upon comparison with a theoretical calculation (not shown).

The position of the I_2 peak was determined as follows. From Fig. 8(c), the I_2 peak has a unique forward-scattering peak in the [113] direction. After acquiring a spectrum $\mathcal{S}_{[113]}$ along this direction and subtracting $\mathcal{S}_{\text{off}}$, the resulting spectrum $\mathcal{S}_{[113]\text{-off}}$ displayed a single-peak I_2 whose energy could be easily determined.

The F 1*s* XPS peak also exhibited CLS's, although they were small enough to preclude easy assignment. We determined from thick films that the XPD modulations (amplitude and position) are virtually identical for F 1*s* and F *KVV* electrons.[42,45] This is a consequence of the similar kinetic energies of these electrons (560 vs 650 eV) for Mg $K\alpha$ irradiation. In the analysis that follows, then, we assume that all the observed F 1*s* peaks have the same XPD modulations as the corresponding F *KVV* AED modulations (Fig. 8). Figure 9(a) illustrates the $\mathcal{S}_{\text{on}}$, $\mathcal{S}_{\text{off}}$, and $\mathcal{S}_{\text{on-off}}$ F 1*s* spectra for the same 3-TL film as in Figs. 5 and 8. From the F *KVV* results above, we know that the $\mathcal{S}_{\text{on-off}}$ spectrum is comprised of two peaks due to the

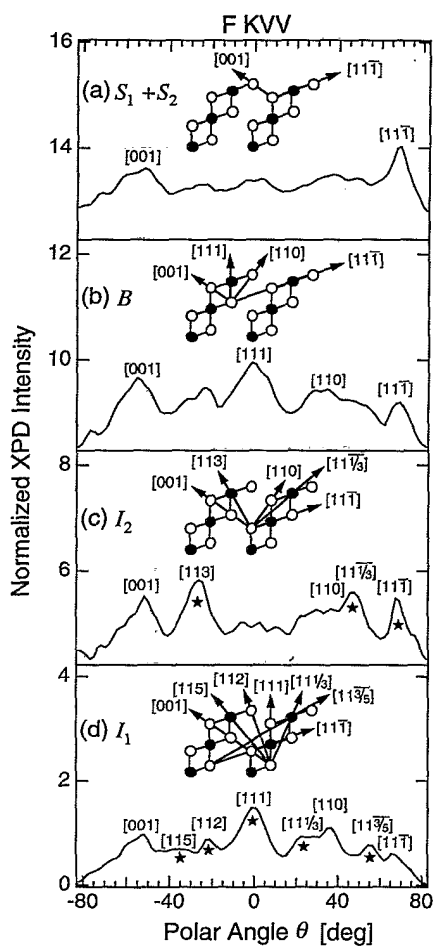

FIG. 8. Experimental F *KVV* AED results for a 3-TL CaF_2 on Si(111) film. (a) Surface F atoms $S_1 + S_2$, (b) bulklike F atoms B, (c) interface F atoms I_2, and (d) interface F atoms I_1. The insets show the corresponding in-plane scattering angles responsible for the forward-scattering peaks in the XPD profiles. Scattering directions, which uniquely distinguish I_1 from I_2 atoms, are shown starred.

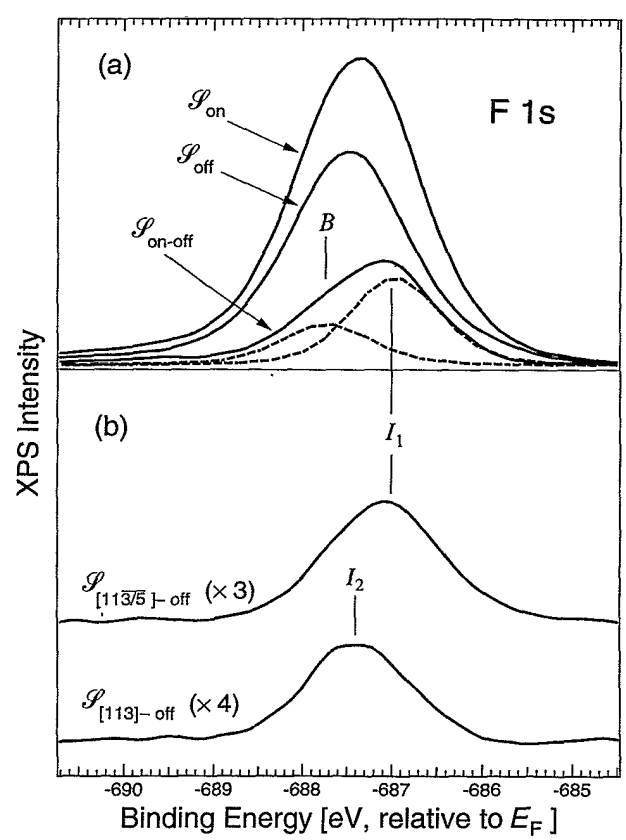

FIG. 9. F 1*s* XPS results for a 3-TL CaF_2 on Si(111) film. (a) $\mathcal{S}_{\text{on}}$, $\mathcal{S}_{\text{off}}$, and the difference spectrum $\mathcal{S}_{\text{on-off}}$, which shows an asymmetric peak consisting of bulk B and interface I_1 components (see Fig. 1), (b) difference spectra $\mathcal{S}_{[11\overline{3/5}]\text{-off}}$ bulk B and $\mathcal{S}_{[113]\text{-off}}$, which are mainly sensitive to I_1 and I_2 interface atoms, respectively.

I_1 and B atoms. Accordingly, the F 1s $\mathcal{S}_{\text{on-off}}$ spectrum has a slight asymmetry. To account for this asymmetry, we have fitted the spectrum to two peaks of splitting ~0.75 eV. From the XPD results presented below, we assign the larger component $\mathcal{S}_{\text{on-off}}$ to be due to the interface atom I_1, while the smaller component is due to the bulk atom B. This is in spite of the fact that electron attenuation should make B larger than I_1 in $\mathcal{S}_{\text{on-off}}$. A possible reason for this is that the forward scattering is greater for I_1 than for B; a further contribution is that the electrons from bulk atoms have an additional intrinsic loss channel that is unavailable to electrons from the interface.

The assignments of B, I_1, and I_2 F 1s peaks are facilitated by CR-AED as suggested by the F *KVV* results in Fig. 8. We observe that the I_1 atom has a unique forward-scattering peak at the angle $\theta=+58°$ (labeled $[11\overline{3/5}]$ in Fig. 8), while similarly, the I_2 atom has a unique forward-scattering peak along $\theta=39°$ ([113]). Therefore, we acquired XPS spectra $\mathcal{S}_{[11\overline{3/5}]}$ and $\mathcal{S}_{[113]}$ at these two angles. Relative to the off-axis spectrum $\mathcal{S}_{\text{off}}$, these spectra showed enhancements at the energies of the I_1 and I_2 peaks; the difference spectra $\mathcal{S}_{[11\overline{3/5}]\text{-off}}$ and $\mathcal{S}_{[113]\text{-off}}$, which show this enhancement, are given in Fig. 9(b). The $\mathcal{S}_{[11\overline{3/5}]\text{-off}}$ is similar to the $\mathcal{S}_{\text{on-off}}$ spectrum, except that the peak is more symmetric, retaining the feature to lower binding energy. This confirms the assignment of this peak to the I_1 atom. The $\mathcal{S}_{[113]\text{-off}}$ spectrum shows a single peak, shifted 0.35 eV to lower binding energy relative to B, which we have assigned to the I_2 atom.

Finally, we consider the position of the surface F 1s signals. In Fig. 9(a), $\mathcal{S}_{\text{off}}$ is slightly displaced to higher binding energy compared to $\mathcal{S}_{\text{on}}$. As before, this indicates that the unmodulated surface signal has higher binding energy than the remaining atoms. However, we cannot rule out the presence of additional surface intensity to lower binding energy in approximately the same position as I_1. This is because the relative forward-scattering enhancements β and ι of B and I_1 are unknown; the observed displacement of $\mathcal{S}_{\text{on-off}}$ may be accounted for if ι is just slightly greater than β. For this reason, we have not presented $\mathcal{S}^*$ data for F 1s, nor have we determined SCLS's for F 1s, except that the absolute values of the shifts are less than about 0.5 eV.

C. Surface modification experiments

The previous sections report the use of CR-XPD and CR-AED to identify surface core-level shifts. We have also studied the SCLS's after modifying the film surfaces in two different ways.

First, the surface Ca atoms may be converted to a bulklike environment by adding an overlayer of SrF_2. We first prepared and characterized a 4-TL CaF_2 film as above, and then covered it with ~1.5 TL's or SrF_2 grown at 400 °C. In this structure, the surface Ca atom's site becomes essentially bulklike and hence its emission S overlaps the signal of the B atom. This is illustrated in the upper part of Fig. 10(a), where we compare off-axis Ca $2p_{3/2}$ spectra acquired from the as-grown and SrF_2-exposed films (normalized to the same intensity to compensate for the attenuation caused by the overlayer). A similar result was observed in Ca *LMM* spectra (not shown). Furthermore, we found that the 1.5-TL SrF_2 cap is crystalline and maintains the same orientation ("type-B") as the underlying CaF_2 lattice. This was demonstrated by analysis of CR-XPD of the two Sr 3d components observed from the first and second SrF_2 TL's.

Second, we studied CaF_2 SCLS's after oxygen adsorption onto our surfaces (possibly in the form of H_2O or OH) due to the residual gases in the vacuum chamber. Changes in the surface core-level intensities were accompanied by a gradual buildup of oxygen 1s photoemission intensity. This adsorption reaction is quite efficient, since a significant coverage may be observed after 10–20 h in a cryopumped system at pressures of 8×10^{-11} Torr.

Off-axis spectra for Ca 2p immediately after growth, after oxygen exposure, and the difference spectrum, are presented in the lower part of Fig. 10(a). The corresponding F *KVV* spectra are presented in Fig. 10(b). We observe a reduction of the surface Ca 2p and F *KVV* signals (evidenced by a dip in difference curves); simultaneously, both Ca 2p and F *KVV* spectra acquire broad

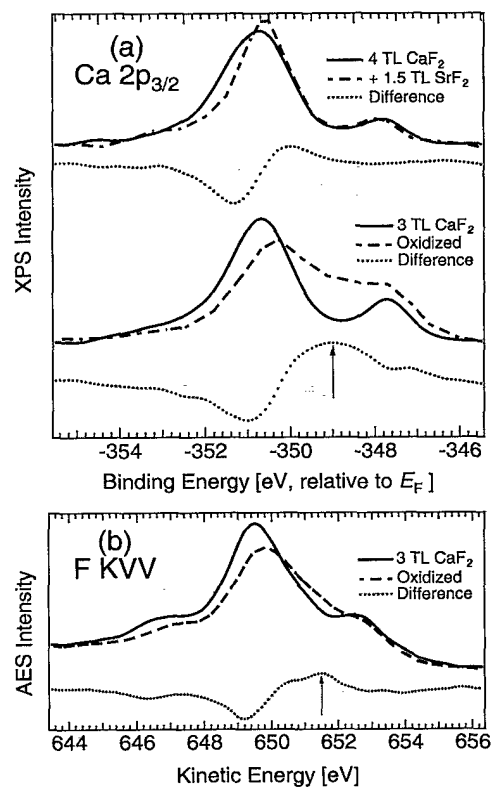

FIG. 10. XPS results shown the effect of surface modification of CaF_2/Si(111) films. (a) Ca $2p_{3/2}$ spectra for (upper) an as-grown 4 TL, followed by ~1.5-TL SrF_2 deposition, and the difference spectrum, and (lower) an as-grown 3-TL film, after oxygen exposure, and the difference spectrum. (b) F *KVV* Auger spectra as grown, after oxygen exposure, and the difference spectrum. The difference spectra show the removal of surface Ca, F components and the appearance of new components indicated by the vertical arrows.

chemically shifted components S' (indicated by the arrows in Fig. 10). For Ca $2p$, the new component is easily seen between the bulk and interface peaks, but for F *KVV* it overlaps with the I_2 component. The net intensity before and after oxygen adsorption in both cases is about the same, implying that the oxygen species adsorbs to the surface rather than reacting to replace surface fluorine atoms.

D. Buried vs exposed ICLS's

The growth mode of CaF_2 on Si at our growth conditions is unusual in that 2-TL-thick islands are nucleated atop the reacted interface layer; these 2-TL islands merge to completely cover the solid, after which layer-by-layer growth begins.[26] Before the islands completely cover the reacted interface, both buried and unburied ICLS's are present, and we have been able to measure the relative binding energies. Additional mechanisms also lead to simultaneous buried and exposed interfaces; for lower flux rates, higher substrate temperatures, or higher substrate step densities, we observe that islands grow atop the Si-Ca-F layer. For all of these conditions, we were able to distinguish CLS's from exposed and buried interface atoms, with similar results. The structures are very similar to the one illustrated schematically in Fig. 1.

Figure 11(a) presents $\mathcal{S}_{\text{on-off}}$ and $\mathcal{S}^*$ spectra for Ca $2p$ in such an islanded layer. A nominally 2.5-TL CaF_2 film was deposited at the relatively slow growth rate of 5 Å/min. The resulting structure consisted of ~4-TL islands covering ~35% of the reacted Si-Ca-F layer, as determined by XPD and XPS.[26,27,45] Similar to the flat film (Figs. 3 and 4), the $\mathcal{S}^*$ spectrum displays a surface signal S, but in contrast to the flat film, the $\mathcal{S}^*$ spectrum displays a peak due to exposed interface Ca atoms I_0 in addition to the surface signal S. We determined the I_0 CLS (relative to I) to be 0.2 ± 0.05 eV, which is an average value obtained for several films of similar morphology.

Figures 11(b) and 11(c) show similar results for F *KVV* and F $1s$ atoms for the same film. Both of these spectra also show new interface components I_0 corresponding to the uncovered interface F atoms. The I_0 CLS's were determined to be 0.84 ± 0.3 and 1.30 ± 0.25 eV for F *KVV* and F $1s$, respectively (averaged over a variety of samples).

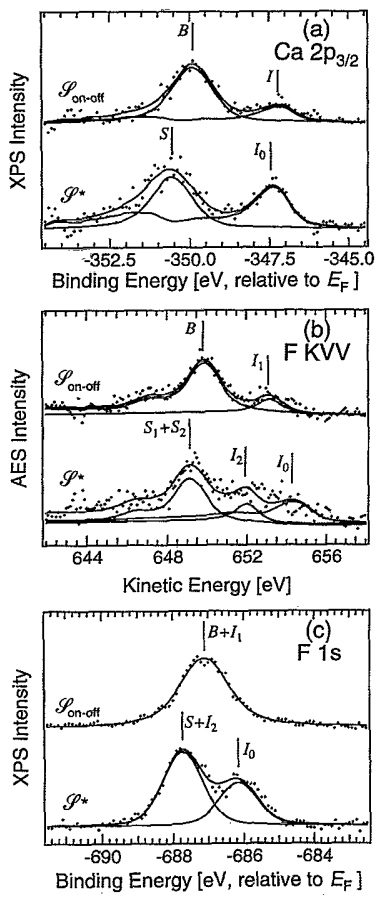

FIG. 11. XPS spectra from a CaF_2 film consisting of islands ~4-TL average height covering ~35% of the Si-Ca-F layer. Spectra $\mathcal{S}_{\text{on-off}}$ and $\mathcal{S}^*$ (sensitive to buried and exposed atoms, respectively) and fitted peaks are shown for (a) Ca $2p_{3/2}$, (b) F *KVV*, and (c) F $1s$. The peak assignments correspond to the buried and exposed atomic sites illustrated in Fig. 1.

E. SrF_2 CLS's

Similar surface and interface core-level shifts to those observed in CaF_2/Si films are also present in SrF_2/Si films. The extra-atomic contributions to these shifts depend strongly on the interatomic distances in the film. To investigate this dependence, we measured SCLS's in SrF_2 films on Si (111). While the chemical bond between SrF_2 and Si(111) is similar to that of CaF_2 and Si, the increased lattice constant creates strain in the films, so that strain should play the dominant role in any differences between CaF_2 and SrF_2 films.

Figure 12 shows the identification of surface, bulk, and interface Sr $3d$ and F *KVV* peaks [Figs. 12(a) and 12(b), respectively]. The film was grown under the same conditions as the 4-TL CaF_2 film. By analyzing the XPS peak heights and CR-XPD modulation amplitudes (using the method of Refs. 26 and 45), we determined the morphology to be ~6-TL islands converging ~50% of the reacted Si-Sr-F layer. This is in contrast to the CaF_2 films, which were almost completely uniform for this growth condition, and is due to the much larger lattice mismatch between SrF_2 and Si (6.8%) than between CaF_2 and Si (0.6%). This large lattice mismatch might drive the system to create islands in order to relieve strain by allowing the bulk islands to relax to their natural lattice constant. This relaxation was confirmed by LEED measurements, where we observed two lattice constants differing by ~8%: from the relaxed SrF_2 islands and from the commensurate Si-Sr-F regions in between the islands.

The SCLS's were found to be 0.63 ± 0.04 eV for Sr $3d$ and 0.64 ± 0.08 eV for F *KVV*. The peak assignments were confirmed using CR-XPD and also by the surface oxygenation. The measurement of the interface positions is difficult for this particular film, since the unburied interface peaks I_0 dominate the observed interface peaks.

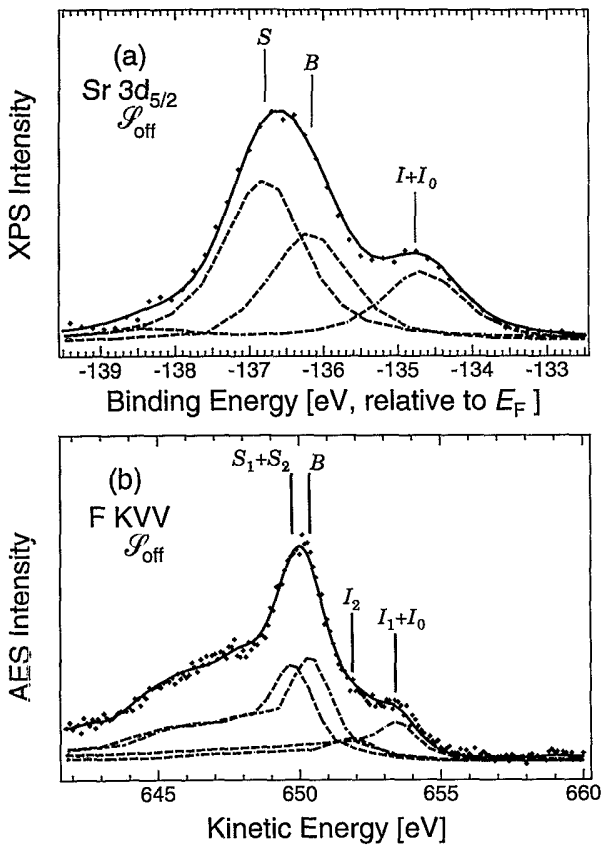

FIG. 12. XPS spectra from a SrF_2 film consisting of islands ~6-TL average height covering ~50% of the Si-Sr-F layer. Off-axis spectra $\mathcal{S}_{off}$ and curve fits for (a) Sr $3d_{5/2}$ showing surface S, bulk B, and interface I_0 and I components (see Fig. 1), and (b) F KVV showing surface S_1+S_2, bulk B, and interface I_2 and I_1+I_0 components. The weak Si $2p$ plasmon loss peak at ~133 eV has been subtracted from (a).

This makes it difficult to measure splittings between buried and unburied interface components; therefore, the fits were performed with a single peak representing both buried and unburied atoms. Preliminary measurements, though, indicate very similar buried-exposed splittings as were obtained for CaF_2.

IV. DISCUSSION

To test the model of CLS's, it is important to measure both Auger and photoelectron shifts, since these are linearly independent combinations of the initial- and final-state effects [Eqs. (1) and (2)]. Agreement between theory and experiment for both ΔE_{PE} and ΔE_{AE} implies agreement for both $\Delta\Phi_M$ and ΔR. We have therefore acquired both Auger and photoelectron shifts wherever possible; in general, good agreement between theory and experiment is obtained. In cases where theory disagrees with experiment, we use the measured CLS's ΔE_{PE} and ΔE_{AE} to invert Eqs. (1) and (2); this yields experimental measurements of ΔR and $e\Delta\Phi_M$, which give insight into the nature of the observed shifts.

Throughout the following, theoretical and experimental CLS's are summarized in Tables I (CaF_2) and II (SrF_2). Unless otherwise indicated, the CLS's are each relative to the bulk energies, which have been corrected to include the effect of finite electron escape depth. Since the bulk atoms near the surface have slightly different relaxation energies, the observed binding energy is an average weighted according to the distance of each atom from the surface. This correction was discussed by Chiang, Kaindl, and Mandel,[8] and amounts to ~10% reduction in the theoretical relaxation shifts ΔR.

A. CaF_2 CLS's

Experimental and theoretical CLS's for CaF_2 on Si(111) films are presented in Table I. First we discuss the 8-TL film, which was sufficiently thick to neglect substrate effects. The calculations are for a slightly strained film with lattice constants $a_{\parallel}=1.000$, $a_{\perp}=1.012$ relative to Si (the inclusion of strain will be discussed below). Also, the relaxation energies were corrected for the penetration depth as discussed above. For the 8-TL film, only the Ca $2p$ and F KVV SCLS's are large enough (compared to the linewidths) to give quantitative measurements. The predicted shifts are in good agreement with experiment, including the prediction that the surface F KVV atoms S_1 and S_2 have approximately equal kinetic energies.

The 4-TL and 3-TL films are thin enough that substrate effects must be included to account for all the CLS's. In the theoretical calculations the Si substrate is treated as a continuous medium with dielectric constant $\varepsilon_{sub}=11.7$, and placed a distance $d_i=0.8$ Å from the nucleus of the interface Ca atom. The interface Ca atom I has charge $q_{Ca}=+2$, the same as for the bulk Ca atoms. The interface Madelung shifts were assumed to be the same as at the surface, which was -0.013 eV for the interface F atom I_1, and only 0.31 eV for the interface Ca atom I. This model assumes that there is a negatively charged layer ($1e^-$/atom) between the interface Ca and Si atoms, a point which will be discussed further below. For the 3–4-TL films, we were able to obtain reliable CLS's for Ca LMM Auger and Ca $2p$ electrons both at the surface and interface. At the surface, there is agreement with theory for both Ca shifts; therefore we can conclude that both the initial-state shift $e\Delta\Phi_M$ and final-state shift ΔR for Ca are predicted correctly by our model. For F SCLS's, we could only get reliable measurements for the Auger-electron shifts, so that we can only determine that the predicted combination $e\Delta\Phi_M+3\Delta R$ is in agreement with experiment.

The large energy difference between the interface and bulk Ca $2p$ emission has been attributed in the past to a chemical shift due to interface bonding with the Si lattice.[22,23] The presence of a shifted interface F peak has also been attributed to F-Si bonding.[22] However, we find that the entire F interface shift, and about $\frac{2}{3}$ of the interface Ca shift may be accounted for simply by the extra-atomic effects outlined in Sec. II. Comparing theory to experiment for the 3- and 4-TL films in Table I, we find

the calculation overestimates the Ca *LMM* shift, and underestimate the Ca $2p$ shift. The opposite sign of these discrepancies indicates that the residual chemical shifts alter both the initial- and final-state energies; the discrepancies are small, however, so that the large ICLS is determined preliminary by (extra-atomic) screening from the Si substrate and only secondarily through residual (intra-atomic) chemical shifts.

The chemical state of the interface Ca atom is an important parameter in the calculations discussed above. We modeled the interface Ca as having an ionic charge $q_{Ca}=+2$, which is contrary to the expectation that the absence of an interface F layer reduces the Ca charge to $q_{Ca}=+1$. This is also contrary to the interpretation of near-edge x-ray-absorption fine-structure measurements by Himpsel *et al.*,[46,47] who concluded that $q_{Ca}=+1$. On the other hand, theoretical calculations by Salehpour, Satpathy, and Das[48] show that 80% of the charge density of the extra electronic state is distributed over the first two substrate Si bilayers; this supports $q_{Ca}=+2$. Furthermore, our model rules out large departures of q_{Ca} from $+2$, which would create larger ICLS's than we observe for the F atoms I_1 and I_2, both from the altered Madelung potential near the interface, and from the altered polarizability of the Ca atom. Of these, the latter is the most important. Upon going from the closed-shell configuration $3s^2 3p^6$ to $3s^2 3p^6 4s$, the Ca polarizability in the interface layer would increase by approximately an order of magnitude. We estimate that for each 0.1 electron added to Ca, the F *KVV* I_1 and I_2 electrons display additional ICLS's of ~ -1.4 and ~ -0.7 eV, respectively. Even in the absence of all of the Si relaxation, a value of $q_{Ca}\sim 1.8$ is sufficient to account for the entire observed F *KVV* ICLS's. Placing the Si at a reasonable distance from the CaF_2 film forces $q_{Ca}\approx +2$.

For the oxygenated 3-TL film, we were able to estimate the altered SCLS's before and after exposure, which are presented in Table I. Equations (1) and (2) may be inverted to yield ΔR and $e\Delta\Phi_M$ in terms of the measured values of ΔE_{AE} and ΔE_{PE}. Performing this inversion for the measurements in Table I, we find that for surface F atoms, $\Delta R\approx -1$ eV and $e\Delta\Phi_M\approx 0.7$ eV. For surface Ca atoms, $\Delta R\approx -1$ eV and $e\Delta\Phi_M\approx -0.7$ eV. These shifts cannot be accounted for by simply covering the CaF_2 with a dielectric layer, since the relaxation energies ΔR and F and Ca are so similar; any simple theory predicts large differences between F and Ca CLS's due to the closer proximity of F to the overlay.

Finally, we compare the unburied to buried interface core levels for a single CaF bilayer and for a bilayer buried under three TL's of CaF_2. For Ca $2p$, the predicted shift between unburied (I_0) vs buried (I_1) Ca atoms is about the same as the SCLS between surface (S) and bulk (B) Ca atoms (~ 0.7 eV). Experimentally, we find a shift of the same direction, but of a much smaller magnitude (0.2 eV). For F $1s$, we expect the I atoms to be more bound ($e\Delta\Phi_M>0$) due to electrostatic interaction with the overlayers and less bound ($\Delta R<0$) due to the additional polarizability of the overlayers. Using Eqs. (1) and (2), the predicted photoelectron and Auger shifts are

$$\Delta E_{F1s}=e\Delta\Phi_M+\Delta R$$
$$=-1.05+0.53=-0.52 \text{ eV (theory)}, \quad (13a)$$

$$\Delta E_{FKVV}=e\Delta\Phi_M+3\Delta R$$
$$=-1.05+1.59=0.54 \text{ eV (theory)}. \quad (13b)$$

From the measurements $\Delta E_{F\,1s}=-1.30$ eV, $\Delta E_{F\,KVV}=-0.84$ eV, we can invert Eqs. (1) and (2) to determine the experimental shifts $e\Delta\Phi_M=-1.5\pm 0.5$ eV and $\Delta R=0.23\pm 0.3$ eV. Although the overall agreement with experiment is somewhat poor, the signs of the predicted shifts $e\Delta\Phi_M$ and ΔR are correct. We observed with XPD that the exposed interface Ca layer had the same XPD pattern as the surface Ca atom, except that the modulation strength was $\sim 50\%$ weaker for the former case. This observation, along with the observed sharpening of interface XPS peaks upon burial, suggests that the exposed interface layer has a significant disorder in the F atom position. This disorder in the exposed interface layer may account for the deviation between experiment and theory. Rieger *et al.*[22] observed the fluorine $I_0\rightarrow I_1$ shifts and interpreted them as completely due to a structural rearrangement of interface F atoms upon burial (within a model where there are two F and one Ca in the interface). We have shown above that the shifts can mostly be accounted for without such an ordered rearrangement.

B. Strain effects: SrF_2

Table II summarizes the SCLS's measured for the islanded SrF_2 film, which we estimated to have islands of 6-TL average thickness covering $\sim 50\%$ of a Si-Sr-F layer. The SCLS's are for atoms within the islands, so that the measurements may be compared with the 8-TL CaF_2 results. Interestingly, the observed SCLS's for CaF_2 and SrF_2 are identical within the experimental uncertainties. As in the case of CaF_2, the S_1 and S_2 F *KVV* shifts remain unresolved.

It is surprising that the measured SCLS's for SrF_2 and CaF_2 are so similar. The increased number of electrons on the Sr atoms should lead to greater polarizability and hence greater relaxation energies R. Furthermore, the tetragonal strain induced by the large SrF_2/Si lattice mismatch alters the computed Madelung energy $e\Phi_M$. Evidently, these effects must nearly cancel so that the overall SCLS's remain the same. To explore these effects further, we considered the effect of tetragonal strain on the SCLS's.

The normal and planar strains in tetragonally strained films are related by

$$e_\perp=-Ae^\parallel, \quad (14)$$

where A depends on the elastic constants, and has the value $A=0.958$ for bulk CaF_2 and 0.880 for bulk SrF_2.[49,50] The fluoride lattice constants relative to Si may then be expressed as

$$a_\perp=-Aa_\parallel+m(1+A), \quad (15)$$

where $a_{\parallel,\perp}$ are the lattice constants of the film in units of the substrate lattice constant, and the lattice mismatch m is 1.006 for CaF_2 and 1.068 for SrF_2. In principle, only a finite range of $a_\parallel$ may be found for a system, constrained by the lattice mismatches both at room temperature and at the growth temperature. Between room temperature and all growth temperatures used in this paper, the isolated fluoride lattices are larger than the Si lattice; therefore the smallest possible value of $a_\parallel$ is 1 (pseudomorphic growth). Since the fluorides have a larger thermal-expansion coefficient than Si, the largest possible value of $a_\parallel$ is given not by the room-temperature mismatches but instead by the larger mismatches at growth temperature: 1.025 (1.08) for CaF_2 (SrF_2). This would be the case for a film fully relaxed to the fluoride lattice constant at the growth temperature. Such large tetragonal strains have been observed both for CaF_2 and SrF_2 on Si(111); the persistence of the growth temperature mismatch at room temperature has been attributed to interface defects, which pin the overlying lattice while the film cools.[49]

The tetragonal distortion affects both the Madelung and relaxation calculations by altering the atomic coordinates in Eqs. (3) and (7). The relaxation calculation is affected in a second way: consistency is required between the polarizabilities α_+, α_-, and the dielectric constant ε_∞, which enters the calculation through **P** [Eq. (9)]. For bulk ionic crystals, which are not tetragonally distorted, consistent values of α_+, α_-, and ε_∞ are compiled in the literature; in the strained films discussed below, these parameters may change due to compression or expansion of atomic orbitals. For these calculations, however, we assume that strained layers have the same polarizabilities as unstrained layers, and we estimate the dielectric constant from the Clausius-Mosotti relation

$$\varepsilon_\infty = \frac{1+2(4\pi\alpha_{\text{tot}}/3v)}{1-(4\pi\alpha_{\text{tot}}/3v)}, \qquad (16)$$

where α_{tot} the total polarizability of the CaF_2 or SrF_2 molecule, and v is the volume per molecule in the presence of strain. For CaF_2, we use $\alpha_+ 0.979$, $\alpha_- = 0.759$ as above, while for SrF_2 we use $\alpha_+ = 1.542$, which was derived assuming the same fluorine polarizability as for CaF_2 and by applying the known dielectric constant of SrF_2 to Eq. (16).

Figure 13 shows the predicted CaF_2 and SrF_2 SCLS's (solid and dashed lines, respectively) as a function of the lateral lattice constant $a_\parallel$. The bulk relaxation part of the calculation has been corrected for the finite electron escape depth as discussed above. The normal lattice constants are constrained by Eq. (15). It is important to note that most of the dependence on $a_\parallel$ in the figure is due to variations in the Madelung potential; ΔR varies by at most 10% over the indicated range, while $\Delta\Phi_M$ can vary by 100% over the same range. The most consistent value of the lateral lattice constant with our data is $a_\parallel \approx 1.08$, for which (i) the predicted Sr 3*d* shift agrees with the experimental measurements, and (ii) the F *KVV* shifts are both equal, although the predicted shift is somewhat smaller than the observed SCLS. For CaF_2, on the other hand, the theoretical SCLS's do not vary much over the relatively limited range of allowed lattice constants, so that we cannot easily distinguish the lateral lattice constant from the SCLS's.

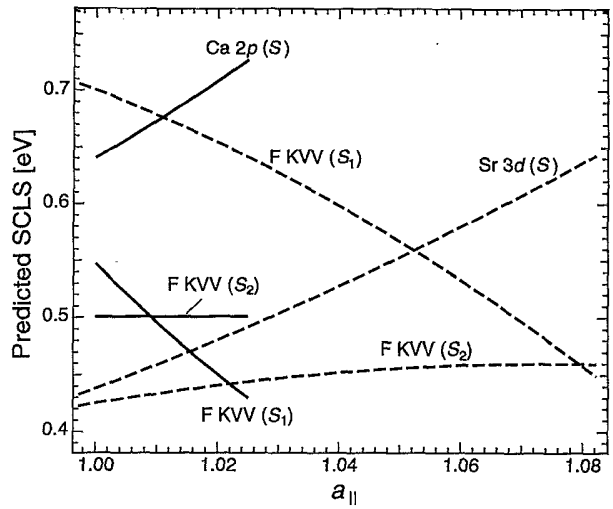

FIG. 13. Predicted CaF_2 (solid) and SrF_2 (dashed) SCLS's for strained films, relative to bulk values (corrected for finite escape depth). Shifts are calculated as a function of $a_\parallel$, the lateral lattice constant relative to the Si substrate. The normal lattice constant $a_\perp$ is constrained as described in the text.

The film strain was measured independently. We observed with LEED that all SrF_2 films thicker than approximately one layer are relaxed to $a_\parallel \approx 1.08$, which is in agreement with our interpretation above. This indicates that the films are under tensile strain, consistent with our earlier study with LEED and x-ray standing-wave fluorescence[51] as well as with ion-channeling measurements.[50] This means that the growth temperature mismatch is retained after cooling to room temperature; interfacial defects prevent the relaxation of overlayer atoms from $a_\parallel \sim 1.08$ to $a_\parallel \sim 1.068$.[49] The theoretical SCLS's for $a_\parallel = 1.08$ from Fig. 13 have therefore been used in Table II.

For CaF_2, on the other hand, we had assumed pseudomorphic growth ($a_\parallel = 1$) in Table I (compressive strain), which is supported by the absence of additional LEED spots, by x-ray scattering results[43,52] on similar films showing $a_\perp = 1.013$ [so that from Eq. (13) $a_\parallel = 1$], and by plane-view transmission-electron microscopy studies, which show no Moiré fringes at these thicknesses.[43]

V. SUMMARY AND CONCLUSIONS

The relationship between atomic structure and core-level spectroscopy was examined for thin ionic insulator films of CaF_2 and SrF_2 on Si(111) by measuring surface core-level shifts and comparing them to an electrostatic model where all the observed shifts are due to geometric, or extra-atomic effects. The assignment of the surface peaks was confirmed with x-ray photoelectron diffraction and also by surface modification. In our model, the two

principal effects are the electrostatic Madelung potential at the core hole and the polarization response of the insulator to the core hole. We found that this model is adequate to describe the observed surface shifts without resorting to intra-atomic or chemical shifts at the surface. We also found that even at the interfaces between the insulators and substrate, where strong chemical interactions are expected to occur, that the electrostatic model accounts for most of the observed shift. This is because the electronic interface state's charge density is distributed through the upper Si layers, where they may be easily incorporated into a continuum dielectric layer. These results illustrate the relative importance of the relaxation response in modeling the core-level shifts in ionic insulators.

We included strain due to mismatch between film and substrate lattice constants into our model. Within our model, we were able to show that the SrF_2 films' lateral lattice constant is greater than the natural lattice constant of the SrF_2 crystal, a result which is consistent with our LEED measurements.

We also demonstrated tha the XPD technique is not only useful for gaining structural information of films, it is also useful for enhancing the effective resolution available from the XPS technique alone.

ACKNOWLEDGMENTS

This work was supported by the National Science Foundation (Contract No. DMR-9196216) and by the Department of Energy (Contract No. DE-AC03-76SR00098). E.R. was partially supported by the U.S. Department of Education.

*Present address: Advanced Light Source, MS 2-400, Lawrence Berkeley Laboratory, Berkeley, CA 94720. Electronic address: ERotenberg@LBL.GOV

†Present affiliation: Department of Physics, University of Oregon, Eugene, OR 97403.

[1]W. F. Egelhoff, Jr., Surf. Sci. Rep. **6**, 253 (1987).

[2]*Photoemission in Solids I: General Principles,* edited by M. Cardona and L. Ley (Springer, New York, 1978).

[3]*Practical Surface Analysis by Auger and X-ray Photoelectron* Spectroscopy, edited by D. Briggs and M. P. Seah (Wiley, New York, 1983).

[4]C. S. Fadley, S. B. G. Hastrom, M. P. Klein, and D. A. Shirley, J. Chem. Phys. **48**, 3779 (1968).

[5]P. H. Citrin and T. D. Thomas, J. Chem. Phys. **57**, 4446 (1972).

[6]D. E. Parry, Surf. Sci. **49**, 433 (1975); **54**, 195 (1976).

[7]R. E. Watson, J. W. Davenport, M. L. Perlman, and T. K. Sham, Phys. Rev. B **24**, 1791 (1981).

[8]T.-C. Chiang, G. Kaindl, and T. Mandel, Phys. Rev. B **33**, 695 (1986).

[9]W. G. Wilke, V. Hinkel, W. Theis, and K. Horn, Phys. Rev. B **40**, 9824 (1989).

[10]F. Bechstedt, R. Enderlein, and D. Reichardt, Phys. Status Solidi B **118**, 327 (1983).

[11]D. K. G. de Boer, C. Haas, and G. A. Sawatsky, Phys. Rev. B **29**, 4401 (1984).

[12]B. W. Veal and A. P. Paulikas, Phys. Rev. B **31**, 5399 (1985).

[13]Eli Rotenberg and M. Olmstead, Phys. Rev. B **46**, 12 884 (1992).

[14]W. Mönch, Solid State Commun. **58**, 215 (1986).

[15]V. Hinkel, L. Sorba, and K. Horn, Surf. Sci. **194**, 597 (1988); W. G. Wilke, V. Hinkel, W. Theis, and K. Horn, Phys. Rev. B **40**, 9824 (1988).

[16]R. Liu, C. G. Olson, A.-B. Yang, C. Gu, D. W. Lynch, A. J. Arko, R. S. List, R. J. Bartlett, B. W. Veal, J. Z. Liu, A. P. Paulikas, and K. Vandervoort, Phys. Rev. B **40**, 2650 (1989).

[17]R. Courths, J. Noffke, H. Wern, and R. Heise, Phys. Rev. B **42**, 9127 (1990).

[18]L. T. Hudson, R. L. Kurtz, S. W. Robey, D. Temple, and R. L. Stockbauer, Phys. Rev. B **47**, 10 832 (1993).

[19]P. Kietz, C. A. Ramos, and P. K. Hansma, J. Vac. Sci. Technol. B **10**, 741 (1992).

[20]Eli Rotenberg, J. D. Denlinger, U. Hessinger, M. Leskovar, and M. A. Olmstead, J. Vac. Sci. Technol. B **11**, 1444 (1993).

[21]P. W. Tasker, J. Phys. (Paris) Colloq. **49**, C6-488 (1980).

[22]D. Rieger, F. J. Himpsel, U. O. Karlsson, F. R. McFeely, J. F. Morar, and J. A. Yarmoff, Phys. Rev. B **34**, 7295 (1986).

[23]M. A. Olmstead, R. I. G. Uhrberg, R. D. Bringans, and R. Z. Bachrach, Phys. Rev. B **35**, 7526 (1987).

[24]M. A. Olmstead and R. D. Bringans, Phys. Rev. B **41**, 8420 (1990).

[25]R. M. Tromp and M. C. Reuter, Phys. Rev. Lett. **61**, 1756 (1988).

[26]J. D. Denlinger, E. Rotenberg, U. Hessinger, M. Leskovar, and M. A. Olmstead, Appl. Phys. Lett. **62**, 2057 (1993).

[27]J. D. Denlinger, E. Rotenberg, U. Hessinger, M. Leskovar, and M. A. Olmstead (unpublished).

[28]U. Hessinger, J. D. Denlinger, E. Rotenberg, M. Leskovar, and M. A. Olmstead (unpublished).

[29]W. F. Egelhoff, Jr., CRC Crit. Rev. Solid State Mater. Sci. **16**, 213 (1990).

[30]S. A. Chambers, Adv. Phys. **40**, 357 (1991).

[31]C. D. Wagner, Faraday Discuss. Chem. Soc. **60**, 291 (1975).

[32]G. Hohlneicher and H. Pulm, J. Electron Spectrosc. Relat. Phenom. **37**, 209 (1985).

[33]J. C. Wang, Phys. Rev. B **22**, 2725 (1980).

[34]M. Kumagai and T. Takagahara, Phys. Rev. B **40**, 12 359 (1989).

[35]N. F. Mott and M. J. Littleton, Trans. Faraday Soc. **34**, 485 (1938).

[36]C. R. A. Catlow, M. Dixon, and W. C. Mackrodt, in *Computer Simulation of Solids,* edited by C. R. A. Catlow and W. C. Mackrodt (Springer, New York, 1982).

[37]P. A. Schultz and R. P. Messmer, Surf. Sci. **209**, 229 (1989).

[38]M. Leskovar, U. Hessinger, J. D. Denlinger, Eli Rotenberg, and M. A. Olmstead (unpublished).

[39]For CaF_2 (SrF_2) the splitting and ratio are 3.5 eV and 0.53 (1.75 eV and 0.67).

[40]J. D. Denlinger, Eli Rotenberg, Uwe Hessinger, M. Leskovar, and M. A. Olmstead, in *Common Themes and Mechanisms of Epitaxial Growth,* edited by P. Fuoss *et al.*, MRS Symposia Proceedings No. 312 (Materials Research Society, Pittsburgh, 1993), p. 207.

[41]Eli Rotenberg, J. D. Denlinger, M. Leskovar, U. Hessinger, and M. A. Olmstead (unpublished).

[42]Eli Rotenberg, Ph.D thesis, University of California, Berkeley, 1993.

[43]G. C. L. Wong, D. Loretto, Eli Rotenberg, M. A. Olmstead, and C. A. Lucas, Phys. Rev. B **48**, 5716 (1993).

[44]C. A. Lucas, G. C. L. Wong, and D. Loretto, Phys. Rev. Lett. **70**, 1826 (1993).
[45]J. D. Denlinger, Ph.D. thesis, University of California, Berkeley, 1993.
[46]F. J. Himpsel, U. O. Karlsson, J. F. Morra, D. Rieger, and J. A. Yarmoff, Phys. Rev. Lett. **56**, 1497 (1986).
[47]F. J. Himpsel, U. O. Karlsson, A. B. McLean, L. J. Terminello, F. M. F. de Groot, M. Abbate, J. C. Fuggle, J. A. Yarmoff, B. T. Thole, and G. A. Sawatsky, Phys. Rev. B **43**, 6899 (1991).
[48]M. R. Salehpour, S. Satpathy, and G. P. Das, Phys. Rev. B **44**, 8880 (1991).
[49]S. Hashimoto, J.-L. Peng, W. M. Gibson, L. J. Schowalter, and R. W. Fathauer, Appl. Phys. Lett. **47**, 1071 (1985).
[50]W. Li, Anthony P. Taylor, and Leo J. Schowalter, in *Mechanisms of Heteroepitaxial Growth,* edited by M. F. Chisholm *et al.*, MRS Symposia Proceedings No. 263 (Materials Research Society, Pittsburgh, 1992), p. 433.
[51]J. D. Denlinger, M. A. Olmstead, Eli Rotenberg, J. R. Patel, and E. Fontes, Phys. Rev. B **43**, 7335 (1991).
[52]C. A. Lucas and D. Loretto, Appl. Phys. Lett. **60**, 2071 (1992).